





Anatomy of a mixed bioclastic–siliciclastic regressive tidal sand ridge: Facies-based case study from the lower Pleistocene Siderno Strait, southern Italy

SERGIO G. LONGHITANO* , VALENTINA M. ROSSI† ,
DOMENICO CHIARELLA‡ , DONATELLA MELLERES§, MARCELLO TROPEANO¶,
ROBERT W. DALRYMPLE** , RONALD J. STEEL†† , ANTONIO NAPPI* and
FABIO OLITA*

*Department of Sciences, University of Basilicata, Campus universitario di Macchia Romana, V.le dell'Ateneo lucano, 10, Potenza, 85100, Italy

†Institute of Geosciences and Georesources, National Research Council of Italy, Via Adolfo Ferrata, 1, Pavia, I-27100, Italy (E-mail: valentina.marzia.rossi@gmail.com)

‡Clastic Sedimentology Investigation (CSI), Department of Earth Sciences, Royal Holloway, University of London, Egham Hill, Egham, TW20 0EX, UK

§DNO E&P, Bادهusgata 37, Stavanger, 4014, Norway

¶Dipartimento di Scienze della Terra e Geoambientali, University of Bari "Aldo Moro", Via Orabona 4, Campus Universitario, Bari, 70125, Italy

**Department of Geological Sciences and Geological Engineering, Queen's University, Bruce Wing/Miller Hall, 36 Union Street, Kingston, ON, K7L 3N6, Canada

††Jackson School of Geosciences, University of Texas at Austin, Austin, TX, 78712, USA

Associate Editor – Anna Pontén

ABSTRACT

Sand ridges, a common feature of modern open shelves, reflect persistent currents and sediment availability under recent transgressive conditions. They represent the largest bedforms in the oceans and, as such, can yield information on long-term oceanographic processes. However, there is a limited number of tidal sand ridges documented from the rock record, examples of regressive tidal sand ridges are scarce and studies describing ridges in straits are even more rare. This study analyses a Gelasian succession within a structurally controlled, tide-dominated strait in the Siderno Basin, southern Italy. The strait connected two wider basins, and accumulated sediments reworked by amplified tidal (bi-directional) currents. A series of tidal sand ridges with superimposed dunes developed close to the south-eastern end of the strait, where bathymetry was deeper and flow expansion occurred. One of the best-exposed tidal sand ridges, 65 m thick, crops out along a *ca* 2 km long cliff. Large-scale, ESE-prograding, seaward-offlapping shingles contain sets of bioclastic–siliciclastic, coarse-grained, cross-stratified sandstones, erosionally overlying upper Pliocene shelf marls and fine-grained sandstones. Cross-strata show angular, tangential and sigmoidal foresets with compound architectures and a SSE migration, i.e. oblique to the main growth direction. Fossil content indicates open-marine conditions. The succession changes abruptly across an erosion surface to non-tidal, highly burrowed mixed siliciclastic–bioclastic fine-grained sandstones, less than 15 m thick. Documented features reflect stages of nucleation, active accretion and abandonment of an individual sand ridge, during a complete cycle of relative sea-level change. The ridge formed during a phase of normal regression, with accretion occurring during an initial highstand and the ensuing falling stage.

During the lowstand the ridge was split into several minor bodies by enhanced tidal currents. The ensuing transgression draped the moribund ridge with tabular strata, whereas final highstand shelf sedimentation reworked the top of the underlying sand body with weak currents.

Keywords Bioclastic, siliciclastic sandstones, Lower Pleistocene, sea-level cycle, Siderno Basin, strait tidal sand ridge.

INTRODUCTION

Tidal sand ridges have for long been described in modern shallow-marine settings (i.e. shelves) and recently recognized in the stratigraphic record (e.g. Allen & Homewood, 1984; Gaynor & Swift, 1988; Surlyk & Noe-Nygaard, 1991; Davis & Balson, 1992; Davis *et al.*, 1993; Mellere & Steel, 1996; Anastas *et al.*, 1997, 2006; Braga *et al.*, 2010; Leva López *et al.*, 2016; Michaud & Dalrymple, 2016; Chiarella *et al.*, 2020). Ridges reveal major net-sediment transport pathways, and the interplay among tidal currents and oceanic currents, storms and waves, reflected in the orientation of the elongated axis and the direction of migration of the superimposed bedforms. Moreover, their occurrence in the rock record is key for unravelling long-term processes that cannot be observed at human timescale in their modern counterparts.

Based on the occurrence of sand ridges in many modern shelves, there is a common consensus in considering these large-scale bedforms as the sedimentary expression of open-marine settings, influenced by oceanographic or tidal currents, Coriolis forcing (Swift, 1975; Snedden & Dalrymple, 1999; Dyer & Huntley, 1999; Reynaud *et al.*, 1999; Berné *et al.*, 2002; Xing *et al.*, 2012) and transgressive reworking of older sediments (e.g. Desjardins *et al.*, 2012; Reynaud & Dalrymple, 2012; Leva López *et al.*, 2016). Sand ridges therefore usually overlie a transgressive surface of marine erosion (Posamentier, 2002; Snedden *et al.*, 2011; Chiarella *et al.*, 2020), have a non-erosive upper boundary that marks their abandonment, and are characterized by clean sandstones and by a compound architecture (Leva López *et al.*, 2016). Modern ridges are very large features, with reported lengths of up to 200 km and thicknesses of up to 50 m (Reynaud & Dalrymple, 2012).

Observations of some present-day examples, such as the Palk Strait between the southern Indian Peninsula and Sri Lanka, the Torres Strait separating northern Australia from

southern Papua New Guinea, and the Strait of Dover between France and the UK, indicate that ridges may also develop along straits, where bottom shallowing, rather than coastal narrowing only, causes local conditions of current convergence and amplification. Case studies documenting tidal sand ridges in the rock record of ancient tidal straits are scarce (e.g. Messina *et al.*, 2014; Chiarella *et al.*, 2020; Leszczyński & Nemeč, 2020) and examples of ridges developed during marine normal to forced regressive stages are rarer (e.g. Wu *et al.*, 2017).

This study presents the results from a field-based sedimentological analysis focused on a spectacular *ca* 65 m thick cross-stratified, mixed bioclastic–siliciclastic succession, exposed along a *ca* 2 km long, laterally continuous outcrop section. Lithofacies and strata geometries, documented through conventional facies analysis techniques integrated with Giga-pan photomosaics, LIDAR (light detection and ranging) scanning and drone photogrammetry, have been interpreted as the sedimentary record of a tidal sand ridge. The stratigraphy of the investigated sand body, also evident in a number of adjacent similar outcrops in the area, indicates stages of nucleation, active accretion and abandonment of the ridges during a complete cycle of relative sea-level change during the Early Pleistocene. In particular, the stage of ridge active migration, corresponding to the switch-on of a tidal circulation in a tectonically-confined strait, occurred during a ‘normal to forced’ regressive phase in the basin. Finally, analysis of oceanographic and palaeogeographic conditions suitable for the development of tidal sand ridges in straits are evaluated.

Tidal straits

Straits are marine passageways in which sedimentation is commonly governed by phenomena of current amplification due to local coastal constriction or bottom shallowing, providing somewhat unusual conditions for sediment transport

and accumulation (Longhitano, 2013). Marine or tidal currents are subject to cyclical phases of acceleration and deceleration during their passage through the narrowest centre, and then expansion as the strait margins enlarge at the two opposing exits (Defant, 1958; Pugh, 1987; Pratt, 1990; Dalrymple, 2010; Longhitano *et al.*, 2012a). In many modern examples, tides occur in phase opposition between the two interconnected basins, generating currents that flow bidirectionally with variable tidal asymmetry in each side of the strait (Vercelli, 1925; Defant, 1940; Androsov *et al.*, 2002). Sediments respond to these hydrodynamics by being distributed in specific depositional zones and forming predictable types of deposits and bedforms. This sedimentary zone partitioning can be recognized in the stratigraphic record of ancient straits, based on a number of diagnostic facies features and depositional architectures (Longhitano, 2013; Longhitano & Chiarella, 2020).

In stratigraphic successions of ancient straits, one of the most distinctive elements is the occurrence of tens of metre-thick cross-stratified sand-rich intervals (e.g. Longhitano & Nemeč, 2005). These typical facies are thought to record zones of bedload convergence commonly separated by a major area of 'bedload parting' and bypass/erosion (e.g. Harris *et al.*, 1995). Vertically stacked cross-strata reflect the migration and superimposition of generations of bedform trains produced by the bed-shear stress exerted by tidal currents on mobile bottom sediments (Allen, 1968; Dalrymple, 1980). Cross-sectional stratigraphic windows oriented parallel to the main direction of sediment transport pathways may reveal diagnostic tidal signatures of bedform complexes, including master erosional surfaces oriented at an oblique angle to the smaller bedforms, herringbone cross-stratification, tidal bundles, rhythmites and reactivation surfaces in sand-size deposits (Longhitano *et al.*, 2012b). Mud, which recurrently occurs in the form of double drapes or muddy intervals in a variety of tide-dominated environments (for example, estuaries, tidal flats, deltas, etc.), is characteristically absent here because of the high-energy setting and the absence of true slack water periods (e.g. Longhitano & Nemeč, 2005; Longhitano & Chiarella, 2020). However, recent studies have documented the occurrence of strait zones where mud can be preferentially accumulated due to local conditions of current depletion (e.g. Longhitano, 2018b). Structures preserved in strait-fill tidal deposits record sedimentation

under the influence of bi-directional flood-ebb currents, occasionally or periodically interplaying with other subordinate factors, such as oceanographic currents, energetic waves and fluvial floods (e.g. Anastas *et al.*, 1997, 2006; Olariu *et al.*, 2012; Rossi *et al.*, 2017; Longhitano, 2018b).

GEOLOGICAL SETTING OF THE CALABRO–PELORITANI ARC AND THE SIDERNO BASIN

The Siderno Basin, together with the Catanzaro, Crati, Crotona and Messina basins in the southernmost part of the Italian Peninsula, is thought to represent one of the extensional depressions that transversally dissected the 'Calabro–Peloritani Arc' (Ghisetti & Vezzani, 1982) during the Plio-Quaternary (Turco *et al.*, 1990; Westaway, 1993; Van Dijk, 1994; Monaco *et al.*, 1996; Van Dijk *et al.*, 2000; Rossetti *et al.*, 2001; Fig. 1A). These basins transitioned into geomorphic straits hosting phenomena of tidal amplification and resulting specific sedimentation roughly during the same time span, i.e. for the entire duration of the Gelasian stage (Longhitano *et al.*, 2012a). The arc forms the uplifted crest of a small orogen presently located in the central Mediterranean and separating the fore-arc Ionian Basin to the east/south-east, from the back-arc Tyrrhenian Basin to the west/north-west (Knott & Turco, 1991). This tectonic setting resulted from the opening of the Tyrrhenian Sea induced by the ongoing north-westward subduction of the Neotethys that started at least at the end of the Palaeogene as a consequence of the collision between the Adria/Africa and Europe Plates (e.g. Malinverno & Ryan, 1986; Patacca *et al.*, 1990; Doglioni, 1991; Doglioni *et al.*, 1999, 2001; Polonia *et al.*, 2011; Carminati *et al.*, 2012; Fig. 1A).

The Siderno Basin is a *ca* 50 km long and 20 km wide extensional area, which developed as an individual tectonic depression onto the thrust orogenic units mostly during the Plio-Pleistocene (Van Dijk *et al.*, 2000). The Basin is bounded by the Serre Massif to the north and the Aspromonte Massif to the south (Fig. 1C). Originally, these massifs represented a unique basement later dissected by important regional eastward-diverging NNE and SSE-oriented strike-slip faults, associated with transversal dip-slip minor structures (e.g. Tripodi *et al.*, 2013, 2018). The Siderno Basin underwent repeated phases of tectonic uplift during the

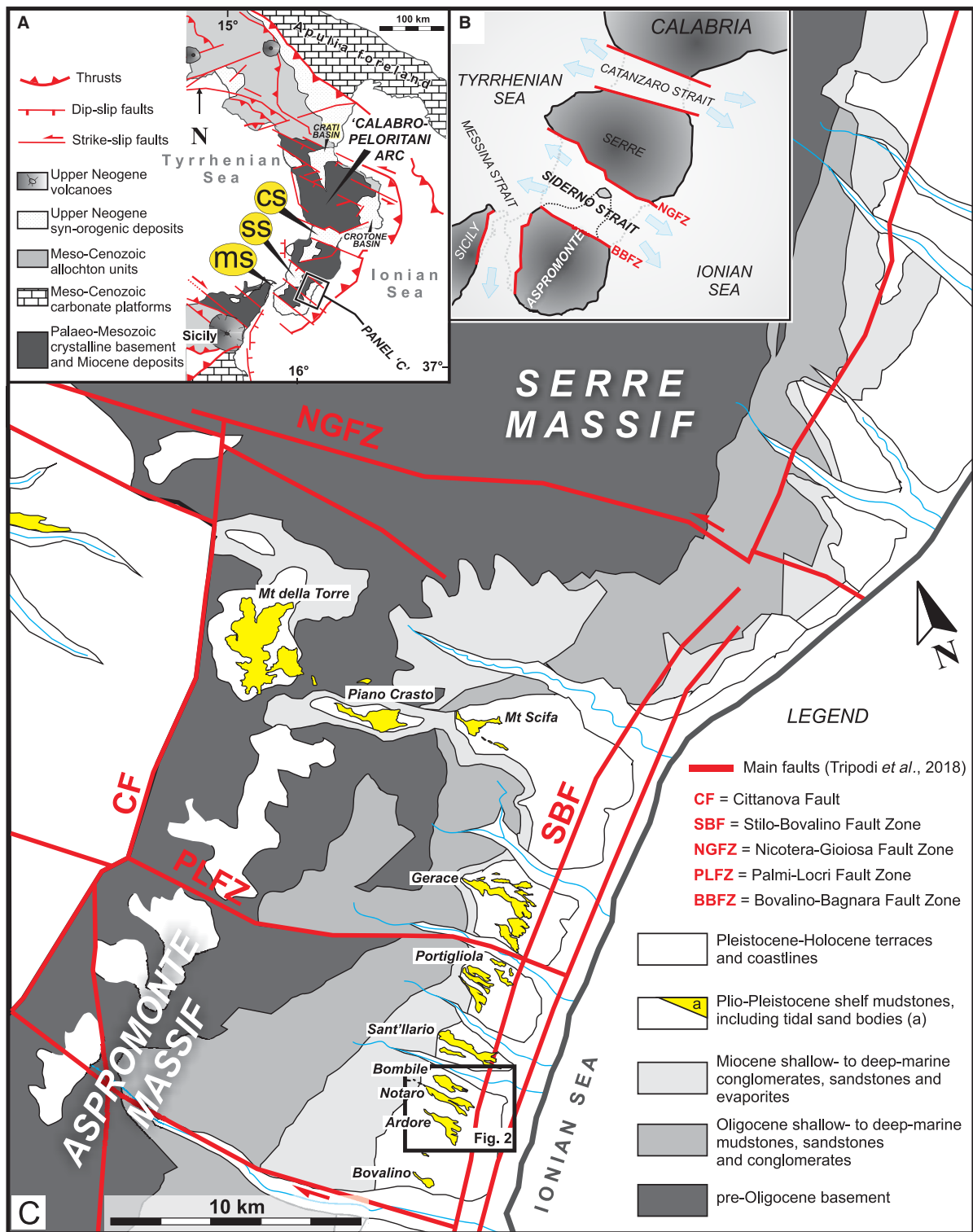


Fig. 1. (A) Structural sketch map of southern Apennines, Italy, showing the Calabro-Peloritani orogen, which originated after the development of semi-regional scale strike-slip zones, delimiting a number of tectonically-controlled straits (cs = Catanzaro Strait; ss = Siderno Strait; ms = Messina Strait) (modified, after Tansi et al., 2007). (B) Palaeogeographic reconstruction of the Pleistocene straits, with the studied sector in the Siderno Strait indicated by the rectangle. Note the occurrence of other adjacent tidal straits. (C) Simplified geological map of the central-eastern sector of the Siderno Basin, showing the main tidal sand bodies in yellow and the area documented in this work (modified from Cavazza et al., 1997).

Quaternary, with a long-term rate of *ca* 2 mm year⁻¹, due to the opening of the adjacent Tyrrhenian Basin (Westaway, 1993). The Siderno Basin changed from a non-tidal seaway into a tide-dominated strait starting at *ca* 2.5 Ma. Tidal conditions persisted for *ca* 900 ka, when a major episode of relative sea-level rise and resulting marine flooding changed it back into a seaway with no significant tidal amplification (Longhitano *et al.*, 2012b, 2021). During the persistence of strait conditions, the tectonic uplift of a central basement high, roughly elongate perpendicular to the main block-faulted margins, separated two major depocentres, one to the west/north-west side of the structure, and the other to the east/south-east (Fig. 1B). After the closure of the seaway, which occurred *ca* 1.3 Ma, a recent (post 700 kyr) stage of tectonic uplift caused the emergence of the basin, accompanied by the development of normal faults dipping towards the Tyrrhenian Sea (Fig. 1A). These latter collapsed the north-western side of the Siderno Basin (Westaway, 1993; Tortorici *et al.*, 1995), causing Quaternary strata to be exposed only in the eastern side of the basin (Cavazza & DeCelles, 1993; Cavazza *et al.*, 1997; Cavazza & Ingersoll, 2005).

The Siderno basin-fill

The Oligocene–Quaternary strata exposed in the area of the Siderno basin form a >2000 m thick succession, non-conformably overlying the late-Hercynian granodiorites, phyllites and paragneiss basement units (Fig. 2B; Amodio-Morelli *et al.*, 1976; Bonardi *et al.*, 1984, 2001; Patterson *et al.*, 1995; Cavazza *et al.*, 1997; Cavazza & Ingersoll, 2005). The lowermost Stilo-Capo d'Orlando Formation consists of carbonates, sandstones, mudstones and conglomerates that accumulated between the Rupelian and the Burdigalian (Bonardi *et al.*, 1980; Cavazza & DeCelles, 1993; Cavazza *et al.*, 1997). The Argille Varicolori Formation unconformably overlies this unit (Fig. 2B) and, based on its characteristic chaotic look, is interpreted as a tectonic mélange composed of red and green shales with local blocks of quartzarenites and marble–limestone emplaced during the Langhian (Amodio-Morelli *et al.*, 1976; Cavazza *et al.*, 1997). The Serravallian–Tortonian interval is recorded in a 450 m thick slope and base-of-slope turbiditic succession overlain by structureless blue claystone, with slumps and channelized conglomerates (Cavazza *et al.*, 1997).

The Messinian succession (Fig. 2B) comprises pre-evaporite limestone and chalk, cobble conglomerates, sandstones and mudstones overlying the Mediterranean-scale unconformity that formed during the dramatic phase of sea-level fall that caused the well-known salinity crisis (Drooger & Broekman, 1973; Manzi *et al.*, 2013; Gorini *et al.*, 2019). During this period, many parts of the basin, as well as the continental shelf of the wider Mediterranean, were exposed subaerially and deeply incised by rivers (Madof *et al.*, 2019). The ensuing transgression is recorded in the *ca* 120 m thick shelf marls of Zanclean age known as the Trubi Formation (Hilgen & Langereis, 1988, 1993). During the Pliocene, the Siderno area began to be tectonically isolated from other adjacent shelf areas of this part of the Mediterranean, taking the form of an individual basin. This stage is recorded in the Monte Narbone Formation (Fig. 2B), which erosionally overlies the Trubi Formation and consists of up to 200 m of well-stratified shelf marlstones and siltstones passing upward into mixed bioclastic/siliciclastic cross-stratified deposits (Cavazza *et al.*, 1997). This latter interval, which includes the section documented herein, exhibits spectacular large-scale cross-stratification that is thought to represent the sedimentary signature of an energetic tidal circulation established in the Siderno Basin during the early Pleistocene (Colella & D'alessandro, 1988; Cavazza *et al.*, 1997; Longhitano *et al.*, 2012b; Rossi *et al.*, 2017), as well as in other adjacent and coeval tidal straits preserved in this sector of the Mediterranean (Longhitano, 2012, 2013, 2018b). The cross-stratified tidal deposits exposed in the Siderno Basin are erosionally overlain by several generations of coarse-grained marine terraces, recording a phase of tectonically-induced forced regression that caused the emergence of the Calabro–Peloritani block during the last 700 kyr (Tortorici *et al.*, 1995) and the demise of the tidal circulation in the Quaternary straits of Calabria (Longhitano *et al.*, 2012a).

Past and present sedimentary dynamics of the Quaternary tidal straits of southern Italy

The strike-slip, block faulting of discrete segments of the Calabro–Peloritani Arc that occurred during the Plio-Quaternary was responsible for the development of a system of coeval multiple straits in southern Italy, including the Catanzaro, Siderno and Messina straits (Fig. 1B).

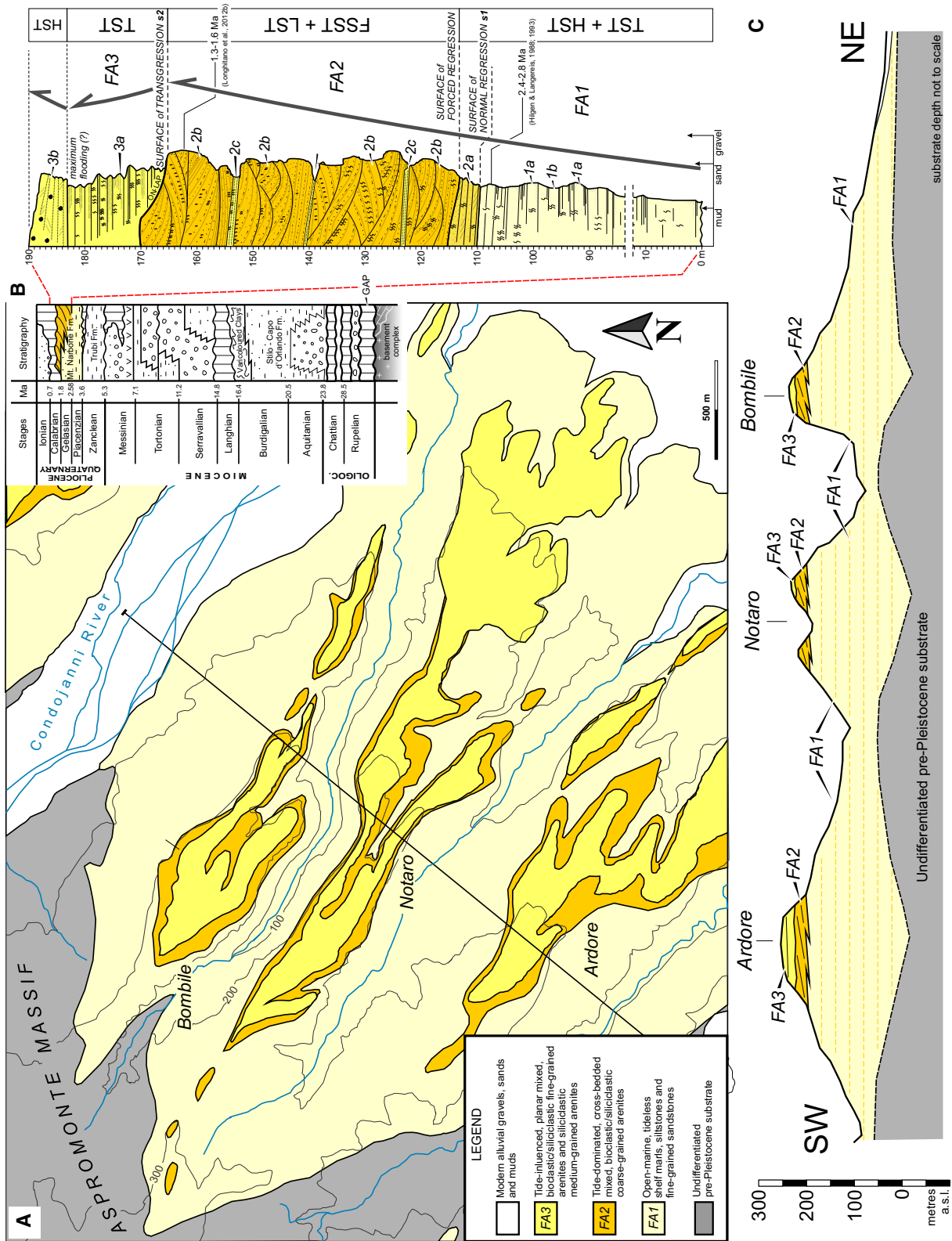


Fig. 2. (A) Detailed geological map of the studied area (see location in Fig. 1C). The present-day exposures of the lower Pleistocene succession form elongate bodies that are oriented parallel to the WNW–ESE orientation of the strait axis. The trace indicates the cross-section in (C). (B). General stratigraphic framework of the Siderno Basin (modified, from Cavazza & Ingersoll, 2005), where the studied interval is expanded into the composite stratigraphic column showing the vertical relationship between the main facies associations and their sequence-stratigraphic interpretation (keys: FA1 to FA3 = facies associations; 1a, 1b, 2a to 2d, 3a, 3b = facies; HST = highstand systems tract; FSST = falling stage systems tract; TST = transgressive systems tract; LST = lowstand systems tract; vertical grey arrows indicate trends of sediment coarsening-upward and fining-upward). (C) Geological cross-section – see location in (A) – showing the distribution of the sedimentary bodies at various locations. The progradation inferred for each section would be the result of an isochronous later shifting of each ridge, as shown in Fig. 3C, and it is represented by the zig-zag line.

These marine corridors provided a hydraulic connection between the Tyrrhenian Basin to the west with the Ionian Basin to the east (e.g. Longhitano, 2013). The Siderno Strait was possibly the largest among all of these passageways (Colella & D'alessandro, 1988; Longhitano *et al.*, 2012a). Water exchange gave rise to currents that underwent hydraulic amplification during their transit at the shallowest/narrowest central zone of the strait (Pugh, 1987; Pratt, 1990). A tidal phase opposition between the Tyrrhenian and the Ionian seas conceivably regulated these hydrodynamics, with cyclicity similar to the tidal fluctuations that presently affect the modern Messina Strait (Androsov *et al.*, 2002). This *ca* 3 km wide passageway separates present-day Sicily from the Italian Peninsula, being continuously subject to up to 3 m s⁻¹ fast currents generated by semi-diurnal tidal inversions (Vercelli, 1925; Defant, 1940). The high tide in the Tyrrhenian Sea corresponds with the low tide in the Ionian Sea, with a water-surface elevation difference of <20 cm (Brandt *et al.*, 1999; Bargagli & Sannino, 2012; Cucco *et al.*, 2016). Although this may appear to be negligible, this gradient is sufficient to transfer large volumes of marine waters through the strait.

The sedimentary partitioning observed in the modern Messina Strait (Longhitano, 2018a) has long been used as an analogue to interpret the stratigraphic successions today preserved onshore Calabria, where the remnants of Quaternary straits are exposed (e.g. Barrier, 1986, 1987; Montenat *et al.*, 1987; Colella, 1996; Chiarella *et al.*, 2012; Longhitano *et al.*, 2012a,b, 2014). In these outcrops, specific types of deposits, as well as distinctive depositional architectures, reveal a process-based correspondence between modern and ancient sedimentary dynamics of tidal straits (Longhitano *et al.*, 2012a, 2014; Longhitano, 2013, 2018a,b). Tidal dunes are the most common bottom feature in the modern Messina Strait and

are dimensionally comparable with many of the cross-stratified facies observed in the outcrops of the ancient straits (e.g. Barrier, 1987; Montenat *et al.*, 1987). However, in the present-day Messina Strait there is no morpho-bathymetric evidence that indicates the occurrence of tidal sand ridges.

METHODOLOGY AND TERMINOLOGY ADOPTED

The main outcrop section was examined first using a series of high-resolution Giga-pan 'photomosaics', which enabled identification of the main architectural elements. The same section was then LIDAR scanned. Sedimentological logging, with detailed observations of the lithology, grain-size and sedimentary structures, was performed along three main accessible outcrops, whereas the remaining three logs presented herein were obtained from the LIDAR and Giga-pan high-resolution digital datasets. The facies analysis of the outcrop was then integrated with petrographic thin-section analysis and the identification of the best-preserved species of benthonic versus planktonic foraminifera. Since a considerable volume of the investigated deposits are arenites of mixed composition, henceforth called 'bioclastic–siliciclastic sandstones', the 'bioclastic/siliciclastic ratio' (*b/s*) and the 'Segregation Index' (*S.I.*; cf. Chiarella & Longhitano, 2012) were estimated for each facies, in order to evaluate the percentage of the dominant clastic component, and the degree of the heterolithic segregation between bioclastic and siliciclastic particles. Cross-stratification analysis was performed by using the geometric models of Rubin (1987). Palaeocurrents were measured on large-scale, medium-scale and small-scale foresets to obtain reliable measurements of true dip-direction. Foreset dip-directions were plotted in rose diagrams using Stereonet® software. The

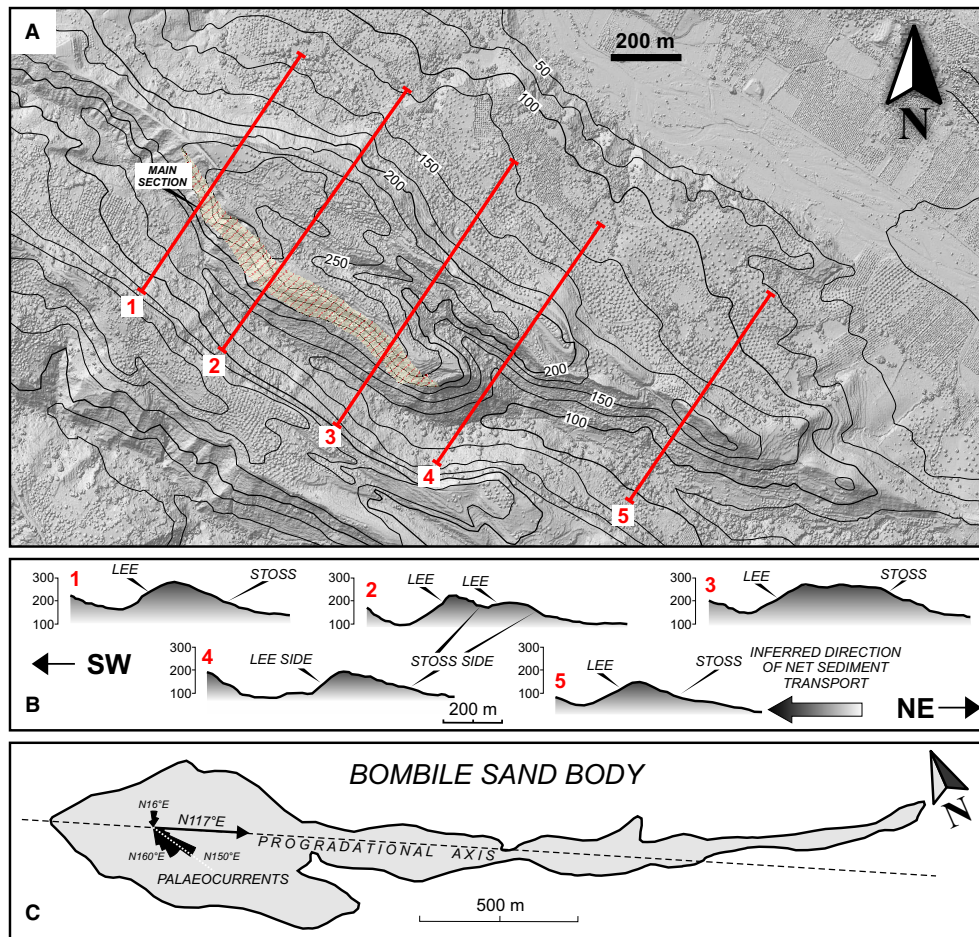


Fig. 3. (A) Digital terrain model-based, topographic relief of the studied section with the main outcrop face (Fig. 4) indicated with oblique lining. (B) Measured cross-sections showing asymmetrical profiles of the investigated relief with a steeper (lee) side always opposite to a gently-sloping (stoss) side, possibly reflecting bedform migration under dominantly unidirectional palaeo-currents or tidal residual with no superimposed unidirectional current. (C) Sketch of the Bombile sand body with the main palaeo-current directions and their orientation with respect to the main elongation axis indicated.

Bioturbation Index (B.I.) was determined using the scale of Taylor & Goldring (1993), together with the main ichnofacies based on the classification provided by Minter *et al.* (2016).

RESULTS

General description of the studied section

The study outcrop section is *ca* 160 m thick and exposed along the southern flank of a *ca* 2 km long and *ca* 700 m wide hill, elongated in a WNW–ESE direction, whose top gently dips towards the east/south-east, from an elevation of 291 to 80 m above sea level (a.s.l.; Figs 2A, 3A

and 4). The hill, where the small town of Bombile lies, is incised by a series of modern shallow river valleys separated by interfluvial elongated downslope (Fig. 3A). These morphological features resemble those of other adjacent hills forming parallel ridges separated by modern river incisions (Figs 1C, 2A and 2C). Relict morphologies are assumed to roughly represent the primary shape of the sand bodies, even though moderately eroded after their recent sub-aerial exposure. This assumption is based on the following observations: (i) the exposed sand bodies are relatively geologically young (i.e. Gelasian) and the area is relatively dry without much river action, therefore it is likely that the sand bodies' original morphology could have

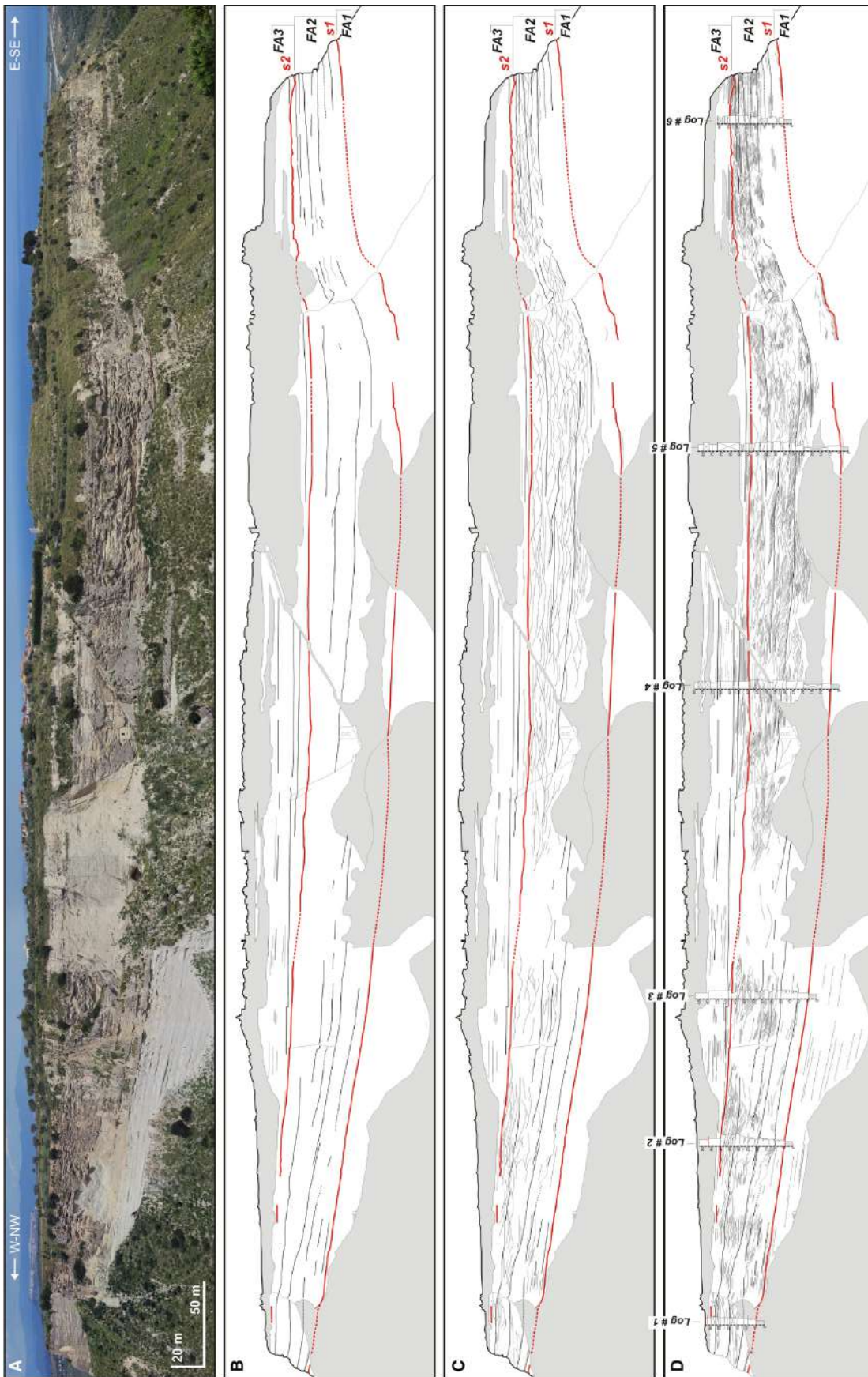


Fig. 4. (A) Photomosaic of the Bombile section oriented WNW-ESE. The outcrop is ca 1200 m in length. (B) First-order discontinuities (s1 and s2) separating the three main facies associations. (C) Second-order surfaces delineating large-scale trough cross-stratification included within FA2. (D) Third-order discontinuities internal to cross-strata indicate foreset architectures. Note the locations of the measured and reconstructed logs (see Fig. 5).

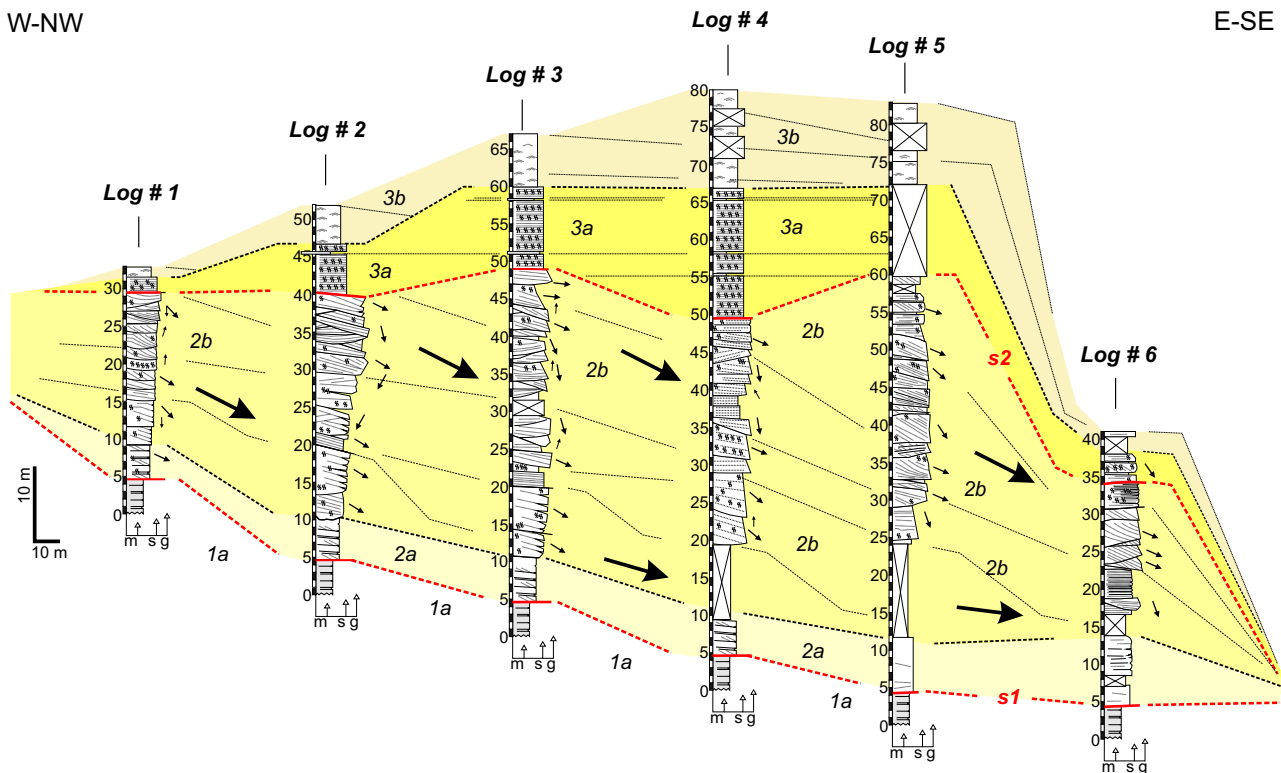


Fig. 5. Correlation of the six measured and reconstructed sedimentological logs. Facies 1a = plane-stratified light-coloured mudstones, marlstones and fine-grained sandstones; Facies 2a = basal plane-parallel to cross-stratified fine-grained bioclastic-siliciclastic sandstones and siltstones, highly burrowed; Facies 2b = large-scale trough-cross-stratified bioclastic-siliciclastic sandstones, highly-bioturbated in places, and including angular to tangential foresets, as well as tidal bundles, rare herringbones and reactivation surfaces; Facies 3a = highly-burrowed, planar-stratified and internally laminated biocalcarenites, lapping against the s2 erosional surface; Facies 3b = structureless or indistinctly cross-laminated texturally mature sands, containing rhodoliths and bivalve fragments. Large arrows indicate main ridge progradation. Smaller arrows indicate direction of migration of superimposed foresets.

been largely preserved; (ii) when analysed from north to south, sand bodies do not show facies differences or proximal versus distal relationships, typical of a prograding dune field (e.g. Bádenas & Aurell, 2001); on the contrary, each of them replicates individually physical characters (for example, grain-size, cross-stratification, stratal patterns, bounding surfaces, etc.) common to all of the examined outcrops; (iii) their in-plan shape, represented by an initial large body dividing into adjacent branches basinward (Figs 1C, 2A and 3C), is another recurrent characteristic that cannot simply be attributed to the present-day erosion but to a primary depositional motif. For these reasons, the authors believe that the original strait-bottom morphology represented by well-cemented coarse-grained ridges and less resistant fine-grained inter-ridges may have very likely conditioned modern rivers to incise the

troughs between the ridges, thereby enhancing the original topography.

Cross-axial sections of the Bombile hill (Fig. 3B) reveal distinctive morphological profiles with opposite flanks having different slope angles, with the south-western side steeper than the north-eastern side (Fig. 3B) and resembling the 'lee' (down-current) and 'stoss' (up-current) side, respectively, of large-scale bedforms. The elongate axis of the Bombile sand body corresponds to a main progradational direction (N117°E) with palaeocurrent trends measured in cross-strata oriented between N16°E and N160°E, showing some bi-directionality but averaging N120°E (Fig. 3C).

Stratigraphy

The exposed sedimentary succession (Fig. 2B) represents the upper Pliocene-lower Pleistocene

stratigraphic interval of the Siderno Basin-fill, known as the Monte Narbone Formation (Cavazza *et al.*, 1997) and more recently assigned to the 'Calcareni di Vinco' Formation (Critelli *et al.*, 2015). The panoramic view of the southern flank of the Bombile Section (Fig. 4A) reveals three main stacked units, here referred to as facies associations *FA1* to *FA3* (Figs 2B and 5), separated by master (first-order) discontinuities and easily distinguishable based on their different colour, reflecting changes in lithology, and by their dominant internal architectures (Fig. 4B). The lowermost facies association (*FA1*) is *ca* 110 m thick and is represented by laterally continuous, white to grey plain-parallel strata, consisting of marls, siltstones and fine-grained bioclastic–siliciclastic sandstones. Based on the presence of well-preserved calcareous nannofossils of the CNPL5 zone (2.4–2.8 Ma) recognized by previous studies (Hilgen & Langereis, 1988, 1993; Longhitano *et al.*, 2012b), this facies association has been ascribed to the Piacenzian–Gelasian interval (Fig. 2B). The overlying facies association (*FA2*; Fig. 4B) lies on a distinctive flat discontinuity (*s1*) and ranges in thickness from *ca* 30 to 60 m (Fig. 2B). Facies Association 2 is characterized by yellowish bioclastic-siliciclastic sandstones and biocalcarenes showing a variety of large-scale stratal geometries separated by cross-cutting lower-rank (second-order) internal discontinuities (Fig. 4C). Stratal geometries include plane-parallel, tabular and trough cross-stratified, and roughly sigmoidal geometries. Angular and tangential foreset bases are considered as third-order surfaces (Fig. 4D). The uppermost facies association (*FA3*) is less well-exposed than the two underlying units due to post-depositional erosion and a diffuse vegetation cover, and consists of 5 to 30 m thick, plain-parallel bioclastic–siliciclastic sandstones, overlying a master discontinuity (*s2*) (Fig. 2B). The section is capped by 10 to 30 m thick discontinuous deposits composed of conglomerates, coarse sandstones and siltstones representing a series of Middle Pleistocene fluvial terraces (Cavazza *et al.*, 1997). Since this study focuses on the Lower Pleistocene interval (Fig. 5), these uppermost deposits are not discussed further.

Description and interpretation of facies associations

Facies Association 1 (open-marine, non-tidal strait)

Description

Facies association 1 (*FA1*) consists of a coarsening-upward succession of light-coloured

mudstones, marlstones and fine-grained bioclastic–siliciclastic sandstones exhibiting plain-parallel, structureless strata (Figs 2B, 6A and 6B) each about 0.6 m thick (*facies 1a*) (Fig. 6C). Towards the top of the succession, 30 to 40 cm thick intercalations of stratified mudstones and fine-grained, structureless or faintly laminated sandstones (*facies 1b*) are more frequent (Fig. 6C). *Facies 1b* contains shell fragments (*Cardium* sp.), isolated shaft burrows (Fig. 6D) and rare shark teeth. In general, the deposits of *FA1* lack signs of tidal influence. The topmost surface (*s1*) bounding this facies association is distinctly exposed along various parts of the Bombile Section (Fig. 4A). It is a conformable surface near the westernmost apex of the section (Figs 6A and 7A), becoming erosional with the overlying *FA2* towards the east/south-east (Fig. 6B).

Interpretation

The deposits forming *FA1* record sedimentation in a non-tidal strait environment, similar to an open-marine shelf dominated by fall-out of fines transported in suspension. Weak and episodic oceanographic traction currents occasionally flowed on the sea floor, as indicated by the rare lamination.

Sediment textures, paucity of stratification and sedimentary structures, and the micro-palaeontological content of the fine-grained deposits of *facies 1a* suggest hemipelagic sedimentation. The structureless and faintly laminated bioclastic–siliciclastic sandstones of *facies 1b* represent tails of density flows moving in a sub-critical regime and transporting fine-grained sediments, as probable distal expressions of high-energy processes generated in proximal sublittoral sectors. The dominant calcareous nature of the sandstones belonging to this facies association implies a general low rate of siliciclastic input to the basin and/or a distal (shelf) environment. However, the coarsening-upward and thickening-upward bioclastic–siliciclastic sandstone intercalations in the uppermost interval (Fig. 6A) suggest a regressive trend and an initial phase of shallowing.

Facies Association 2 (actively accreting tidal ridge)

Description

The sedimentary deposits included within Facies Association 2 (*FA2*) form the middle interval of the studied section and comprise the main body of the tidal ridge (Figs 4A, 5 and 7A). *FA2* exhibits a variable thickness ranging from 20 m near the west-north-west apex of the

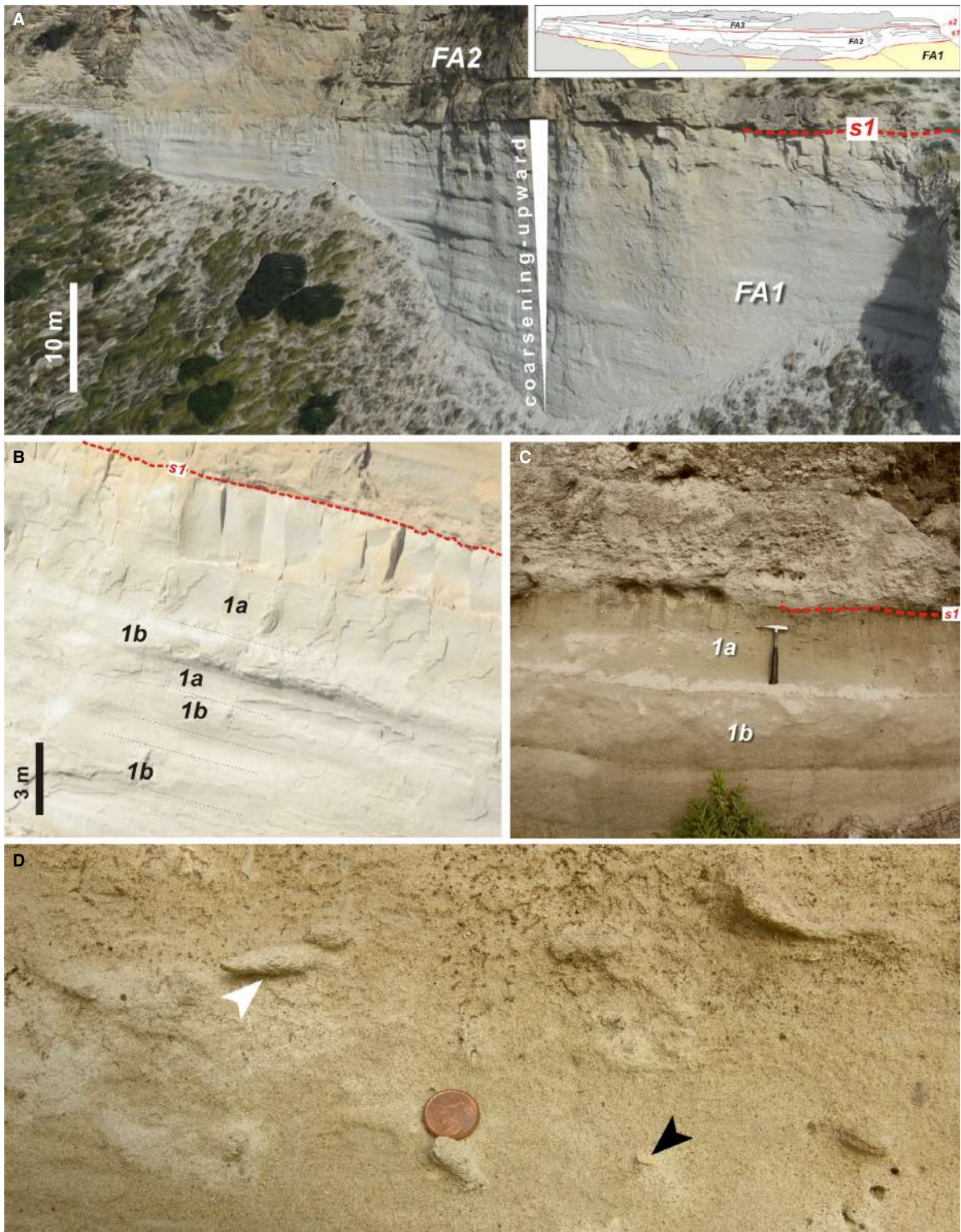


Fig. 6. Outcrop pictures of Facies Association 1 (FA1). (A) Drone photograph showing the distinctive aspect of Facies 1a and Facies 1b and surface s1. (B) Plain parallel light-coloured mudstones, marlstones and fine-grained sandstones (Facies 1a) alternating with highly burrowed plane-parallel to cross-stratified fine-grained sandstones and siltstones (Facies 1b). (C) and (D) Close-up details, revealing these facies right below the s1 contact with the overlying FA2 and the occurrence of burrowing (white arrow indicates probable *Ophiomorpha*, black arrow indicates a mollusc shell) (hammer is 35 cm long; coin as scale is 2 cm in diameter).

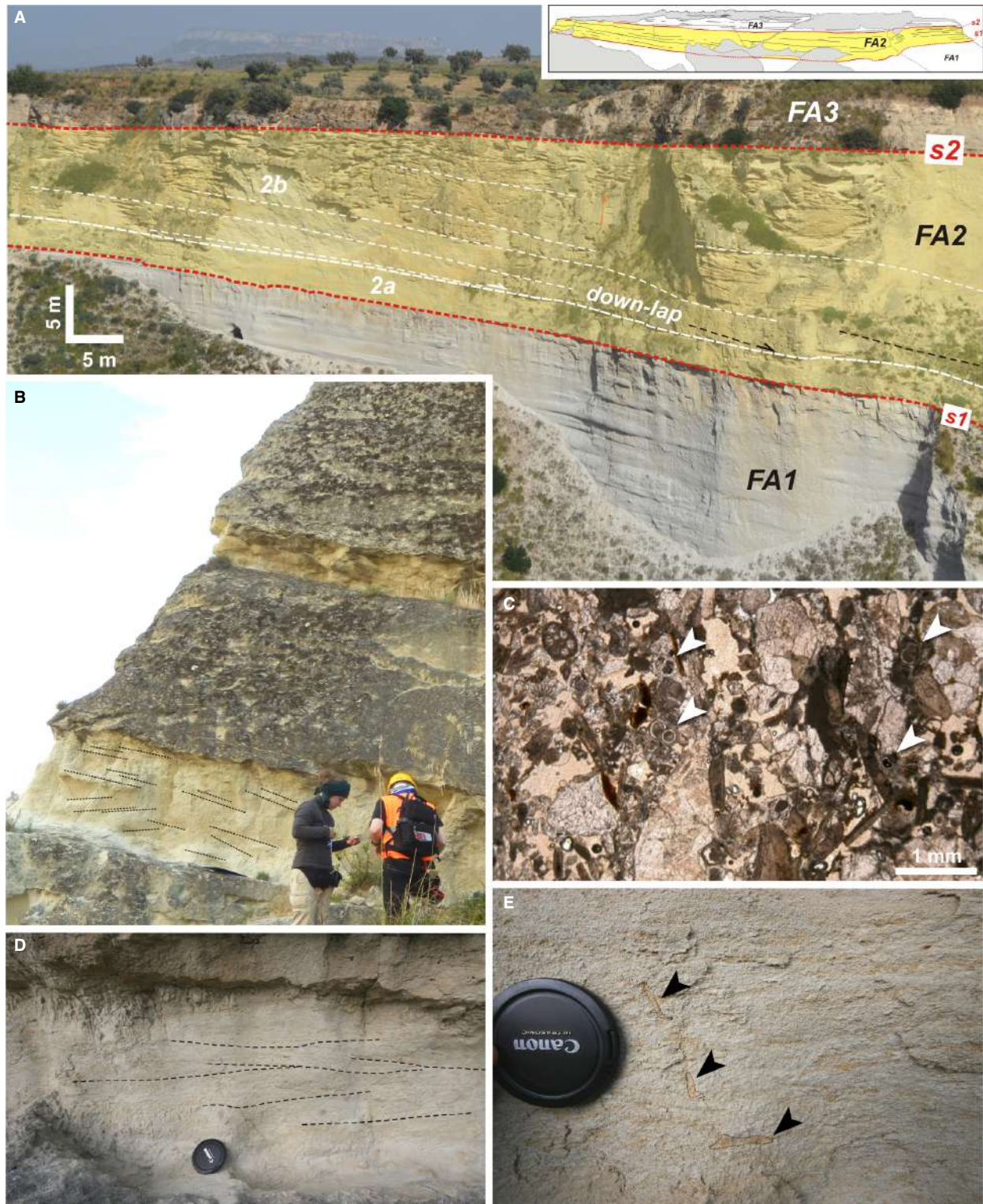


Fig. 7. Outcrop pictures of Facies Association 2 (FA2). (A) Drone photograph showing the down-lap of Facies 2b over the deposits of Facies 2a. (B) Outcrop of Facies 2a showing internal cross-stratification and tabular basal surfaces. People for scale are *ca* 1.6 m tall. (C) Thin section micro-photograph showing the presence of planktonic foraminifera (arrows) in a mixed bioclastic-siliciclastic sandstone comprising several skeletal fragments. (D) Detail of Facies 2a showing indistinct low-angle cross-lamination and (E) *Ophiomorpha* bioturbation (arrows) (camera cap is 8 cm in diameter).

Bombile Section, up to 80 m east/south-eastward, and pinching-out again further towards the east/south-east (Fig. 5). FA2 comprises four main facies (*Facies 2a* to *2d*), which have been distinguished based on their predominant internal architecture, relative occurrence along the studied section, and proportion of bioclastic and siliciclastic fractions.

Facies 2a: laminated fine-grained bioclastic–siliciclastic sandstones and siltstones

Textural features and fossil content.

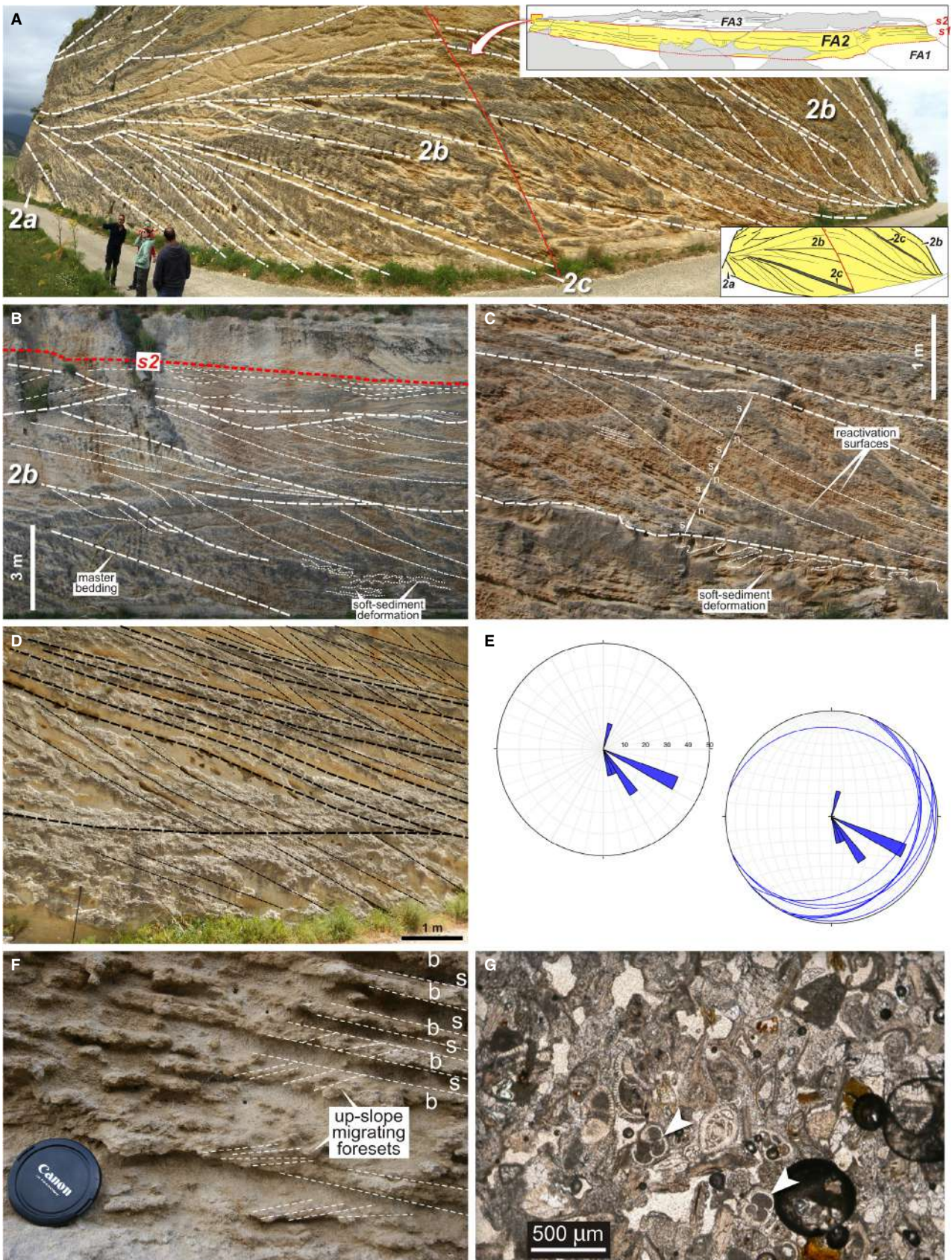
Facies 2a (Fig. 7A and B) consists of whitish mixed, bioclastic–siliciclastic sandstones (b/s ratio $\gg 1$, i.e. containing a relative percentage of siliciclastic particles $< 20\%$). The most pronounced depositional architecture exhibited in cross-sectional view is a tabular stratification parallel to *s1* basal discontinuity (Fig. 7B). Internally, indistinct cross-stratification is visible in places, as well as plane-parallel lamination. The siliciclastic fraction consists of very well-rounded clasts of quartz and lithic fragments, whereas the bioclastic fraction comprises skeletal fragments of echinoids and bryozoans, and, subordinately, of gastropods and bivalves (Fig. 7C). Benthonic and planktonic foraminifera are also present (Fig. 7C). *Facies 2a* exhibits a moderate degree of segregation between the bioclastic and siliciclastic particles at the laminae scale, with no apparent order or cyclicity (Fig. 7D). Internally, localized clusters of mud clasts are visible (Fig. 7D and E). The B.I. ranges between 2 and 3, with the most recurrent ichnofossils represented by *Thalassinoides* and *Gostrochaenolites*. At regular stratigraphic intervals (i.e. every 7 to 10 m), 50 to 70 cm thick recessive siltstone intercalations (*Facies 2c*) occur.

Facies 2b: large-scale, trough-cross stratified bioclastic–siliciclastic sandstones

Textural features and fossil content.

This facies erosionally overlies the underlying deposits of *Facies 2a* (Fig. 7A) and it is characterized by a gently-inclined master bedding surface dipping towards the east/south-east, with strata-sets ranging in thickness between 5 m and 7 m that down-lap onto the underlying deposits of *Facies 2a* (Fig. 7A). However, the most noticeable inner architecture is a complex of stacked sets of large-scale cross-strata (Fig. 8A). Individual cross-strata show tangential foresets truncated by concave-up discontinuities (Fig. 8B). When preserved, foresets exhibit sigmoidal geometry internally separated by reactivation surfaces and, in places, by tidal bundles (Fig. 8C). This specific foreset feature occurs systematically, forming cyclical patterns of coarsening-upward and fining-upward lamina-sets (Fig. 8C). The base of the foresets (toesets) is often associated with the presence of soft-sediment deformation structures (Fig. 8B and C). Cross-stratification frequently forms a compound architecture, with superimposed smaller foresets descending along the lee side of larger foresets (Fig. 8D). They indicate a dominant direction of migration towards the south-east (Fig. 8E). Sediments of *Facies 2b* consist of well-sorted, coarse-grained mixed sandstones (Fig. 8F), with a b/s ratio ranging from 1 to $\gg 1$ (i.e. siliciclastic particles between 20% and 40%). The siliciclastic fraction consists of very well-rounded clasts of quartz and feldspar, whereas fragments of molluscs and echinoderms mainly represent the macroscopic bioclastic fraction. Segregation, indicated by high value of S.I., is locally recognized and is highlighted by the separation of the two antithetic components in discrete lamina

Fig. 8. Outcrop photographs of *Facies 2a*, *2b* and *2c*. (A) Road-cut at the WNW edge of the Bombile Section (vertical exaggeration is *ca* 1.5 \times). Master bedding of *Facies 2b* indicates active accretion towards the right, whereas interbeds of *Facies 2c* record momentary stages of sediment starvation. People for scale are *ca* 1.7 m tall. (B) Detail of *Facies 2b* showing tangential foresets truncated by concave-up discontinuities. (C) Reactivation surfaces within individual foreset units are recognizable thanks to internal down-lap of inclined laminae. Foresets also exhibit cycles of coarsening-upward and fining-upward lamina-sets interpreted as neap (n)/spring (s) intervals. Soft-sediment deformations are also present at the toe of large foresets. (D) Example of compound foreset architecture, with small superimposed cross-strata descending along the lee side of larger underlying cross-strata. (E) Rose diagrams (Stereonet[®]) relative to the measurements of palaeocurrents obtained from foreset surfaces. (F) Intensely bioturbated alternation of bioclastic (b) and siliciclastic (s) intervals showing angular and tangential foreset laminae migrating up-slope on inclined master surfaces. Lens cap is 8 cm in diameter. (G) Thin section micro-photograph showing the relatively good degree of sorting of *Facies 2b* made up of a mixed bioclastic–siliciclastic sandstone, whose carbonate fraction comprises planktonic foraminifera (white arrows) and other undefined skeletal grains.



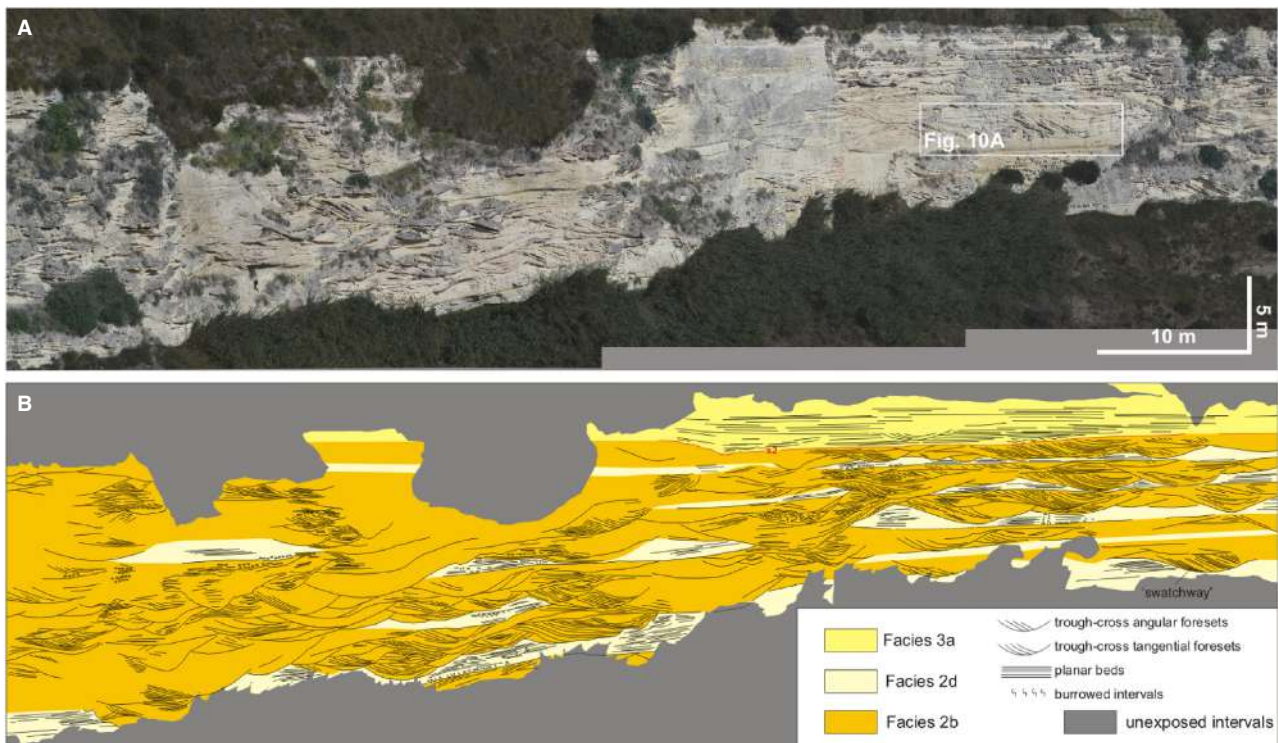


Fig. 9. (A) Panoramic photograph of the central portion of the Bombile Section, showing diffuse trough cross-stratification in a roughly strike-oriented cut. (B) Line-drawing of (A) showing the lateral and vertical relationships among *Facies 2b*, *2d* and *3a* and their internal foreset architectures.

intervals within foreset units, where up-slope migrating 3 to 4 cm thick foresets occur (Fig. 8F). Thin sections reveal an abundance of planktonic foraminifera (Fig. 8G). The S.I. decreases sharply in correspondence with intervals where the bioturbation has secondarily mixed the bioclastic and siliciclastic particles. Bioturbation is widespread (B.I. = 3 to 4) and tends to homogenize and disrupt the primary sedimentological fabric of this facies (Fig. 8F). They have been interpreted by Caruso *et al.* (2011) as a type of echinoid meniscate burrow and infaunal colonization, whose traces appear concentrated along the main foreset surfaces of individual cross sets (Fig. 8F).

Depositional architectures.

Facies 2b is dominated by sets of large-scale trough cross-strata (Fig. 8B and C), although isolated sets of planar cross-strata also occur (Fig. 9A and B). Strata are from 1 m up to 7 m thick, with an average thickness of 2.2 m, and are up to 15 m wide, separated by concave-up erosional surfaces (second-order) with cross-cutting relationships. Internally, foresets show

geometry resembling the ‘scalloped cross-bedding’ of Rubin (1987), i.e. compound cross-stratification with bounding surfaces that cyclically scoop down into previously deposited foresets or into the underlying sediments. Trough cross-strata exhibit three main types of geometrical arrangements or sets (Fig. 10A): (i) sub-horizontal, with the adjacent younger trough eroding the previous one but maintaining the same stratigraphic height (Fig. 10B); (ii) ascending, with the younger trough higher than the previous one (Fig. 10C); and (iii) descending, with the younger trough cross-bed incising the previous one and older strata, but in a lower stratigraphic position (Fig. 10D). These three architectures are part of a continuum, describing ‘ascending to descending’ trajectories in their direction of accretion, where foresets first climb, move sub-horizontally and finally incise downward eroding the underlying strata, in *ca* 50 m of average lateral length (Fig. 10A). Cross-strata geometries are in places cut by U-shaped erosional forms, up to 15 m wide, incising the underlying strata down to 6 to 7 m, with up to 15° steep walls,

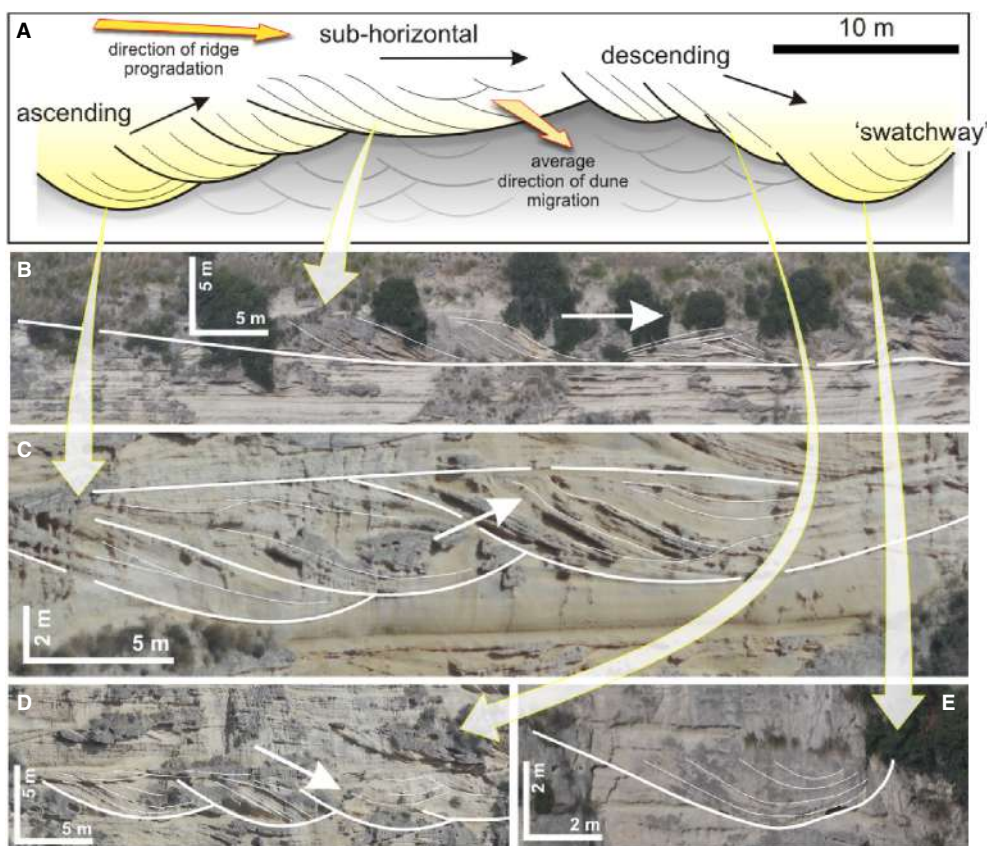


Fig. 10. (A) Trough cross-beds trajectory, as reconstructed from the interval section of Fig. 9A. Foresets are part of a *continuum*, describing sub-horizontal lateral accretion (B), ascendant (C) and descendant (D) path. (E) Spoon-shaped erosional/depositional feature interpreted as a possible swatchway. In all of the outcrop pictures, the average direction of dune migration is somewhat towards the observer, whereas the direction of ridge progradation is towards the right (east/south-east).

and filled by tangential concave-up foreset strata, whose curvature decreases upward (Fig. 10E). Internal foreset geometries range from angular, tangential to sigmoidal, including internal discontinuities (i.e. reactivation surfaces) indicated by laminae pinch out and compound architectures (Fig. 9B). The majority of the foresets (*ca* 92%), which are also the thickest ones, dip in an east/south-east direction. Only a very small proportion points towards the north; consequently, there is a paucity of herringbone cross-stratification in the examined succession.

Facies 2c: highly-bioturbated fine-grained bioclastic-siliciclastic sandstone intercalations
Cross-strata sets of the previous facies are truncated by discontinuities at regular stratigraphic heights, *ca* every 5 to 20 m along the succession (Fig. 11A). Fine-grained Fe-Mn and glauconitic-rich

bioclastic-siliciclastic sandstones, plane-parallel laminated, occur over such surfaces, forming recessive planar intercalations 1.0 to 1.5 m thick and representing *Facies 2c* (Fig. 11B). These deposits include mud clasts (Fig. 11C) and are laterally continuous for some tens of metres but, in places, they disappear due to erosion by the overlying trough cross-strata of *Facies 2b*. Sediments are moderately burrowed by *Ophiomorpha* (Fig. 11D).

Facies 2d: planar stratified bioturbated bioclastic-siliciclastic sandstones
Textural features and fossil content.

The deposits of *Facies 2d* occur scattered along the southern face of the Bombile Section and consist of 0.5 to 1.0 m thick layers that are internally laminated (Figs 9A and 12A to C). In the central portion of the section, where cross-stratified *Facies 2b* prevails, *Facies 2d* occurs only as localized intervals, up to 3 m thick, as partially

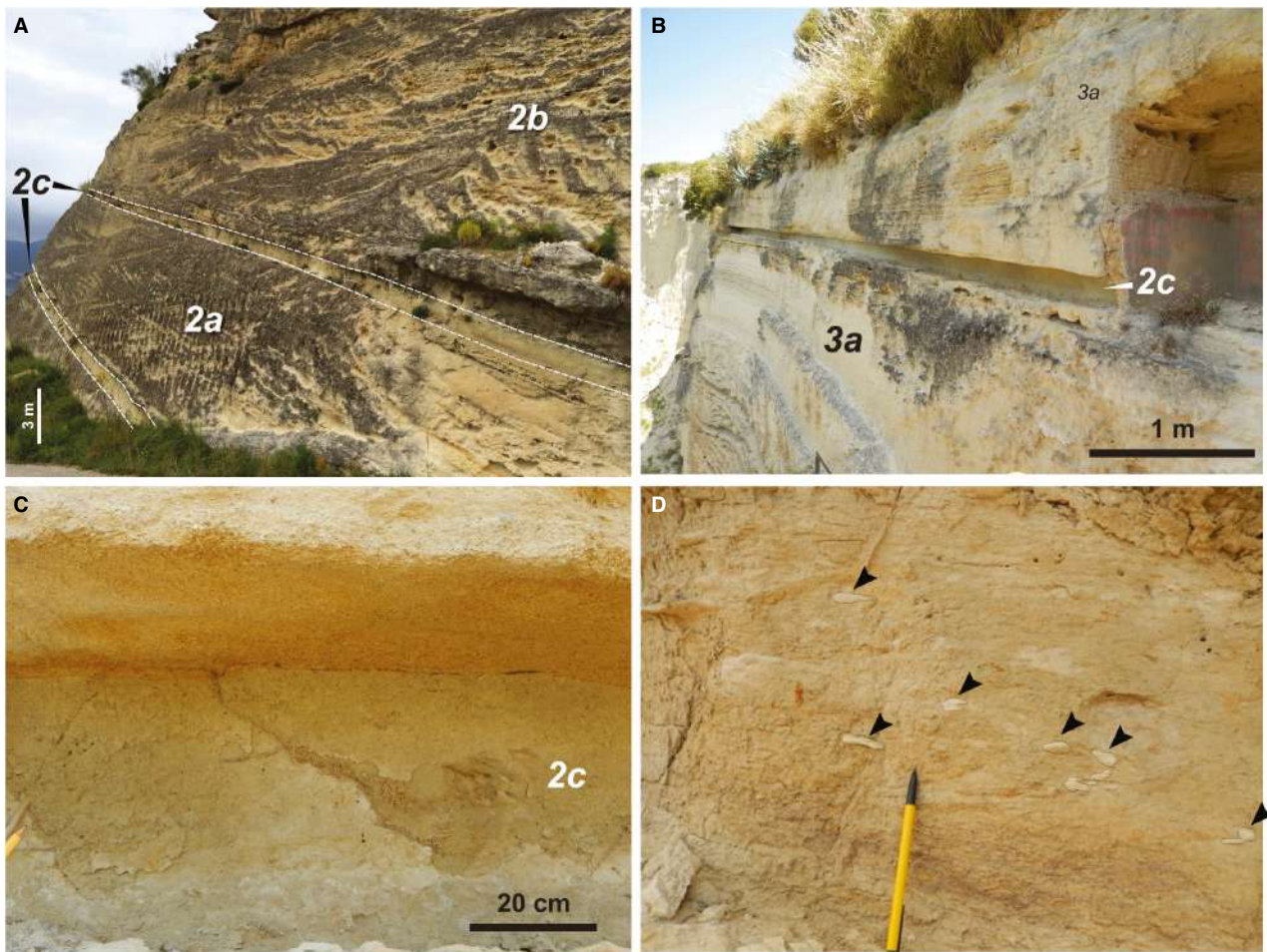


Fig. 11. (A) and (B) Outcrop photographs showing how Facies 2c forms recessive horizons intercalated at quasi-regular stratigraphic intervals within Facies 2a and 3a. (C) and (D) Details of Facies 2c showing no evident structures and isolated *Ophiomorpha* burrows (arrows). Pencil for scale is 15 cm.

preserved remnants bounded by erosional surfaces (Fig. 9B). In the easternmost sector, where large cross-stratification progressively disappears, sediments of *Facies 2d* are more abundant and continuous, forming an uninterrupted succession up to 60 m thick (Fig. 12A). Compositional segregation is still recognizable in localized lamina packages but the primary structures are almost totally homogenized by very diffuse burrowing (Fig. 12D). Bioturbation is widespread (B.I. = 4 to 5), representing the most distinctive feature of this facies. Ichnogenera include small traces of *Thalassinoides* and *Skolithos*. Siliciclastic and bioclastic particles are similar in composition to those described for the previous facies but are characterized by a finer grain-size. The b/s ratio $\gg 1$ led the authors to describe these fine arenites as a packstone

(Fig. 12E) rich in bryozoans, echinoderms and mollusc fragments with interspersed small quartz and schist rounded-clasts. Shells of larger bivalves are diffuse.

Depositional architectures.

The dominant architecture visible in the strata forming *Facies 2d* is a sub-horizontal to gently-inclined stratification, interrupted locally by isolated cross-strata up to 50 cm thick (Fig. 12A and B). In places, stratification dips at a very low angle (*ca* 5° to 6°), generating bounding surface pinch-outs and large-scale low-angle cross-stratification.

Interpretation.

The deposits of Facies Association 2 are interpreted to record the evolutionary progression (i.e.

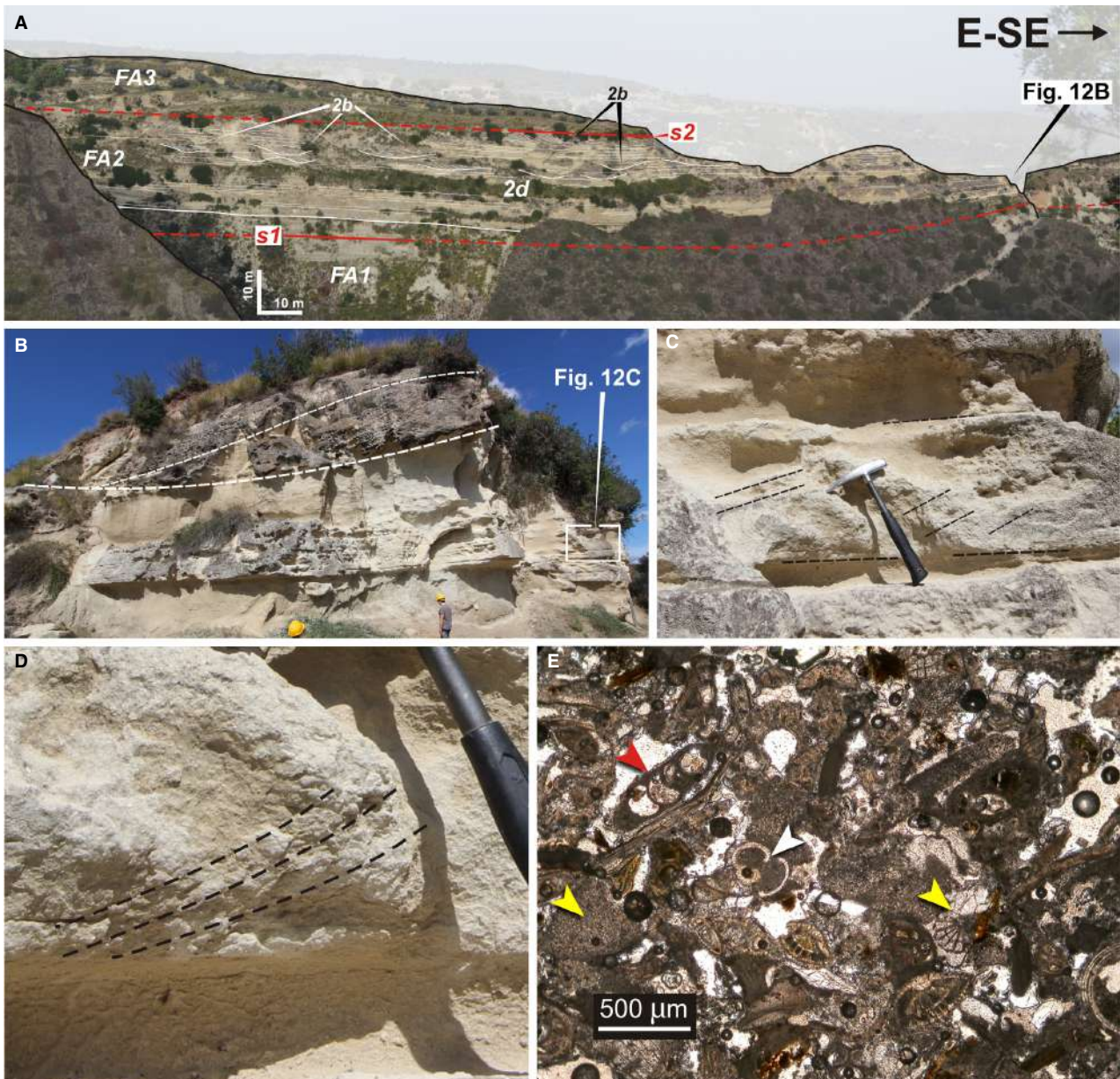


Fig. 12. (A) Terminal, ESE segment of the Bombile Section, showing the flat-lying stratification typical of Facies 2d. (B) Isolated cross-strata are intercalated with dominantly tabular sandstone strata (C), which appear indistinctly cross-laminated (D) (hammer for scale is 35 cm long). (E) Thin section reveals the prevailing carbonate nature of grains, and texturally the rock is a packstone. Among foraminifera, planktonic and benthonic exemplars are indicated with white and red arrows, respectively; bioclastic skeletal fragments belonging to a plate of echinoid (yellow arrow to the left) and a spine of echinoid (yellow arrow to the right) are indicated.

birth and growth) of an individual mixed, siliciclastic-bioclastic tidal ridge, similar to other ridges that are elongate in the same direction and with identical facies, overlying shelf deposits in the eastern side of the Siderno Strait.

Bioclasts within the whole facies association are interpreted to be derived from a heterozoan

carbonate factory (*sensu* James, 1997), and are characterized by light-independent filter-feeders. The scarcity or absence of red algae suggests that carbonate production mainly took place close to, or deeper than, the limit of life of red algae that in the Mediterranean Sea should not exceed *ca* 100 m of depth (Canals & Ballesteros, 1997;

Basso, 1998). However, the presence of a siliciclastic input, the consequence of which is water turbidity due to suspended material, suggests that the local limit of light penetration could have been shallower. In any case, the carbonate assemblage of skeletal fragments of aphotic-biota associated with a relative abundance of planktonic foraminifera indicates that the carbonate factory developed in offshore environments comparable to those of cool-water outer ramps (*sensu* Pedley & Carannante, 2006). All carbonate components appear to be remobilized from their original position and mixed with siliciclasts. However, the local abundance of bioturbation suggests that the biological community lived in the same environments of sedimentation. Therefore, an influx of terrigenous particles could not have inhibited significant *in situ* carbonate production, despite high-hydrodynamic conditions. The concentration of burrowing in discrete intervals within foresets indicates that these deposits were part of an environment characterized by variable rate of sediment accumulation, as is typical within dune fields, where individual bedforms can be more active if compared with interdune areas or troughs. A variable percentage of planktonic foraminifera sinking from the water column enriched the autochthonous (coming from skeletons of biota fragmented and remobilized *in situ*) and parautochthonous (coming from skeletons of biota living in a shallower or different position) carbonate sedimentary fraction of these compositional mixed sediments (*sensu* Chiarella *et al.*, 2017).

The basal sediments comprising *Facies 2a* are interpreted to represent the nucleation of an early-stage, or 'juvenile ridge' of Class I of Snedden & Dalrymple (1999). This facies records an important oceanographic change in the Siderno Basin: an initial low-energy, non-tidal strait turned rapidly into a current-dominated subaqueous (strait) environment, affected by a moderately energetic hydrodynamic regime (Belderson & Stride, 1966; Belderson *et al.*, 1982; Belderson, 1986). Autochthonous to parautochthonous bioclasts and subordinate fine-grained siliciclastic grains, presumably derived from subaqueous reworking of underlying shelf deposits, were mixed to form *Facies 2a* under a current-dominated regime.

The moderate degree of segregation between the siliciclastic and bioclastic components indicates episodic variations in the current competence related to random hydrodynamic processes (for example, storms, oceanographic currents,

etc.), rather than to tidal influence. This non-tidal, but current-reworked setting is inferred by the occurrence of the diffuse but indistinct motifs of cross-stratification and internal plane-parallel lamination suggesting dominance of traction in sediment dispersal mechanisms. The recessive siltstone intercalations would reflect short-term interruptions of the flows and the deposition of fines previously transported away from this area and basinward. The absence of storm-related features (for example, wave-ripples or swaley and hummocky cross-stratification) suggests an average depth located far below storm-wave base (Reineck & Singh, 1980). Basinward wedging-out of master bedding surfaces is indicative of a general progradation along a gently-dipping subaqueous slope with no significant erosion of the underlying shelf strata. This large-scale architecture possibly reflects sedimentation during a late phase of relative sea-level stillstand, preceding a subsequent period of long-term lowering induced by the Aspromonte Massif uplift.

The deposits of *Facies 2b* mark the transition from a current-influenced, non-tidal setting into a tide-dominated strait system, and record the growth of a tidal sand ridge up to its stage of maturity (cf. Leva López *et al.*, 2016). This hydrodynamic change was possibly induced by the onset of a relative sea-level fall, which would have reduced the hydraulic cross-sectional area of the Siderno Basin, turning a non-tidal seaway into a tide-dominated strait. Textures and lithological composition of *Facies 2b* reflect a remarkable increase in the current energy (e.g. McLean, 1990). The mixing of fragments of organisms typical of highly energetic waters with fragments of species adapted to lower-energy environments, suggests erosion and transport of the skeletons of organisms originally populating hydrodynamically more quiet areas, possibly located up-current (e.g. Reynaud & James, 2012; James *et al.*, 2014). Large-scale cross-stratification is believed to record the superimposition of different generations of tidal dunes, migrating under the bed-shear stress exerted by bi-directional currents, affected by a strong tidal asymmetry and modulated in their competence changes (Allen, 1980, 1982; Allen & Homewood, 1984).

The tidal hydrodynamic regime is inferred by the occurrence of a variety of physical structures, including reactivation surfaces, rare herringbone strata, tidal bundles, alternated angular to tangential toesets, as well as simple and compound dune foreset geometries (Fig. 8), preserved within the dune foresets or, at least,

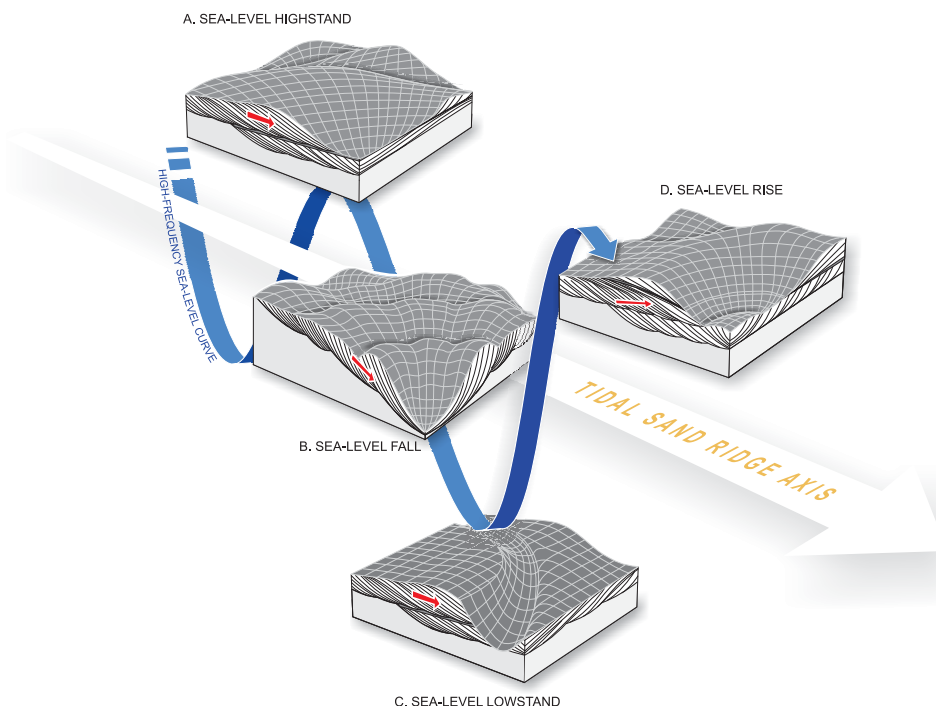


Fig. 13. Varieties of three-dimensional bedforms reconstructed from the observed Siderno cross-stratification (modified, after Rubin, 1987) and indicating styles of lateral accretion controlled by variations in current speed, possibly related to relative sea-level positions. Arrows indicate trajectories of bedform advancement that are: (A) sub-horizontal during stages of relative sea-level highstand; (B) descending during periods of sea-level lowering; (C) sub-horizontal again but dissected by channels or swatchways during stages of sea-level lowstand; and (D) ascending during periods of relative sea-level rise. For simplicity, superimposed smaller dunes with opposite direction of migration, which is typical of tide-influenced settings, are not indicated here.

where they have been protected from homogenizing burrowing (Visser, 1980; Nio & Yang, 1991; Longhitano *et al.*, 2012b; Chiarella, 2016). Soft sediment deformation structures observed at the base of some foresets may indicate local bedform instability and resulting pseudo-plastic collapse along dune lee sides (e.g. Chiarella *et al.*, 2016). The relatively moderate to low values of the S.I. suggest that only a low amount of mixed particles were segregated into separate lamina intervals during low-energetic tidal stages (for example, neap intervals) whereas, for the most part, they were unsegregated during episodes of elevated turbulence of the tidal flows (for example, spring intervals; Fig. 8C; Longhitano, 2011).

Dunes were mostly unidirectional due to a dominant south, south-eastward flowing tidal (ebb) phase influencing the eastern side of the Siderno Basin (Fig. 8E). This basinward growth direction of the main sand body, shown by both the downlap direction and the dominant

palaeocurrents is also key evidence of the regressive character of the tidal ridge. However, the superimposed smaller bedforms, some of them migrating north-westward, would reflect the signature of a subordinate tidal phase.

The depositional architectures observed in the foresets extensively exposed along the Bombile Section (Figs 9 and 10) reflect bedforms undergoing rapid changes in their height indicative of strong and periodical fluctuations in the strength of the tidal flow (Rubin & Hunter, 1982; Rubin, 1987; Fig. 13). The cyclical changes of the accretion pathways observed in a number of large-scale foresets (Fig. 10A) are interpreted to have been imparted by longer-term fluctuations of the current velocity, possibly related to high-frequency and low amplitude sea-level changes acting at Milankovitch timescale (i.e. 41 kyr; Abreu & Anderson, 1998). Sigmoidal foresets migrating horizontally reflect along-crest dune accretion during stages of sea-level stillstand (Fig. 13A). Scalloped foresets showing

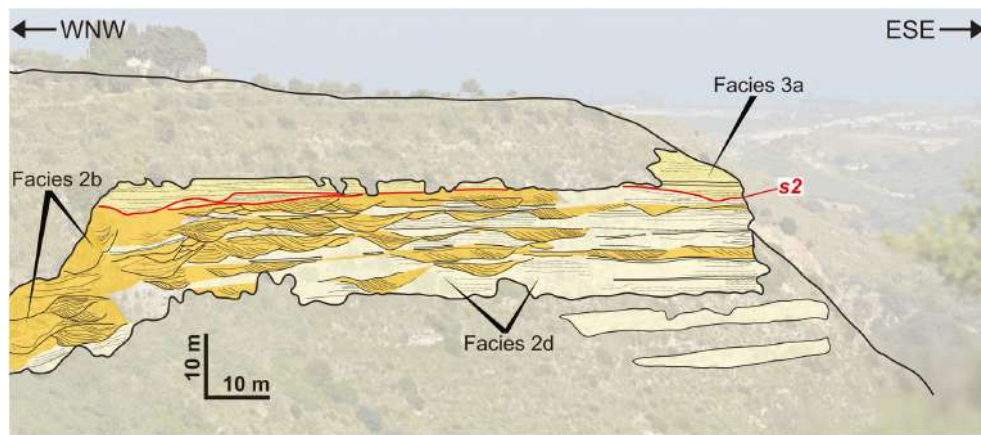


Fig. 14. Lateral relationship between *Facies 2b* and *Facies 2d* observable in the lateral south-east termination of the Bombile Section. Net flow was towards south/south-east (approximately towards the observer).

descending trajectories and eroding underlying strata record dunes moving under accelerated flows due to a stage of relative sea-level lowering (Fig. 13B). Dunes of *Facies 2b* were in places dissected by channels (Fig. 10E), whose geometry is similar to that documented in a transgressive, Holocene (post Last Glacial Maximum) tidal sand bank in the south-eastern Celtic Sea (Reynaud *et al.*, 1999, see fig. 13). These cross-dune deep scours can be related to stages of increased current speed achieved during periods of sea-level lowstand (Fig. 13C). They are interpreted to be incisions very similar to ‘swathways’ observed in estuarine settings (e.g. Dalrymple & Rhodes, 1995) but developed in more distal (shelfal) environments. In particular, these authors refer the genesis of swathways to conditions of local flow constriction exerted by lateral confinement of large dune crests and enhanced at a particular point during a relative sea-level drop (Reynaud *et al.*, 1999). The internal channel-fill tangential foreset geometries record the accretion of smaller dunes along the conduit. Their upward decreasing concavity and width reflects the diminishing energy of the constricted flow and the final channel filling. Foresets with ascending trajectories would reflect stages of relative sea-level rise (Fig. 13D). The occurrence of recessive (finer-grained) but laterally continuous levels at regular intervals in the stratigraphy may indicate short-term episodes of starvation of the active tidal ridge and the temporary switch-off or migration of the carbonate factory responsible for the bioclastic sediment supply to the bedforms (Snedden & Dalrymple, 1999).

The thinner but laterally continuous intercalations represented by the deposits of *Facies 2c* mark periodic episodes of current cessation and inactivity of the tidal sand ridge after stages of active accretion (e.g. Saha *et al.*, 2016). Glauconite, iron-rich and manganese-rich concentrations and shell packages indicate a sudden decrease in the sediment accumulation rate and condensation, and the colonization of the sea floor by infaunal organisms for relatively long periods.

The deposits of *Facies 2d* record sedimentation in areas partially isolated from the major tidal current pathways and are interpreted to represent ridge environments or sub-environments belonging to the dune-field complexes but localized along the troughs of large-scale bedforms or their lateral swales (e.g. Dumas *et al.*, 2005; Messina *et al.*, 2014). In modern dune fields developed in open-shelf current-dominated settings (e.g. Belderson *et al.*, 1982; Belderson, 1986), these zones are characterized by relatively low-energy, where residual flows may transport finer-grained sediments with accumulation rates two or three times lower than the adjacent high-energy sectors where large dunes migrate (Arnott & Southard, 1990). These zones promote conditions for living organisms that prefer low energy environments and whose shell fragments are successively reworked by strong currents and included within the high-energy deposits. In the Bombile Section, sediments of *Facies 2d* occur pervasively between large-scale cross-strata of *Facies 2b* and dominate in the south-eastern (basinward) sector of the section, where, presumably, the primary



Fig. 15. (A) Outcrop of Facies Association 3 (FA3) erosionally overlying Facies Association 2 (FA2) above the widespread surface *s2* (arrows). (B) Different perspective of the same contact visible along the staircase descending over the Bombile Section. (C) Plane-parallel lamination is diffusely present within the tabular strata of Facies 3a. (D) Thin section revealing the presence of planktonic foraminifera (white arrows) within skeletal fragment bioclasts. (E) Topmost part of the Bombile Section showing the erosional contact *s2* (arrows) separating Facies 2b from Facies 3a (dotted red line indicating surface *s2* is intentionally not drawn through the entire image to show the natural aspect of the contact).



Fig. 16. Sedimentary deposits of Facies 3b exposed at the very top of the Bombile Section. (A) Siliciclastic sands showing inclined stratification (person for scale is ca 1.6 m tall) with (B) internal indistinct foresets visible in places (helmet for scale is 22 cm high). (C) Close-up views reveal burrowed horizons (the main traces are indicated with black arrows) and scattered lenses of rhodoliths (white arrows) (hammer for scale is 35 cm long).

dune field of the ridge migrated laterally towards a less energetic fringe. In this portion of the outcrop, large cross-strata are interbedded with the planar strata, forming a lateral transition (Fig. 14), with dunes migrating over the less energetic deposits of *Facies 2d*, indicating the long-term progradational trend of the system.

Facies Association 3 (transgressive moribund tide-influenced ridge)

Description

The deposits included in this facies association represent the topmost strata of the studied outcrop section and consists of two main facies, *3a* and *3b*, for a total thickness ranging from 5 to 15 m. They overlie a widespread, low-relief erosional surface (*s2*, Figs 7A, 12A, 14 and 15A), that dips basinward, incising into the underlying cross-stratified deposits and marking a

change in the general depositional architecture from trough cross-stratification to a dominantly plain-parallel stratification.

Facies 3a: highly-burrowed planar-stratified fine-grained bioclastic–siliciclastic sandstones

Textural features and fossil content.

Facies 3a overlies and laps onto the *s2* discontinuity (Fig. 15A), which erosionally truncates and flattens the underlying large-scale cross-strata (Fig. 15B). This facies is composed of quartz, biotite, feldspar and abundant glauconite grains admixed with fragments of molluscs, echinoderms and bryozoans, as well as red algae and serpulids. The ichnofacies fabric resembles features common to *Bichordites* (Caruso et al., 2011), associated with subordinate *Thalassinoides* and *Skolithos* with a high degree of

bioturbation (B.I. up to 4) (Fig. 15C). Among foraminifera, the planktonic ones exceed 90% (Fig. 15D), with few exemplars of abraded benthonic foraminifera.

Depositional architectures.

Stratification forms plain-parallel horizons that are laterally continuous for hundreds of metres (Fig. 15A) but are indistinctly recognizable at a close distance due to the very intense bioturbation (Fig. 15B). The basal discontinuity on which these deposits sit is a scour surface that dips gently basinward, with local incisions into the underlying cross-stratified deposits (Fig. 15C). Planar strata of *Facies 3a* lap against the steepest segments of this discontinuity, draping, at broader scale, the underlying irregularities (Fig. 15E). The main geometrical trend is thus aggradational to retrogradational, because the higher planar horizons of the deposits of *Facies 3a* climb westward over the slightly deformed back-edge of the underlying cross-stratified tidal ridge deposits.

Facies 3b: structureless, to faintly laminated siliciclastic-rich sandstones

Textural features and fossil content.

Facies 3b consists of apparently structureless but well-sorted medium to fine-grained sands, containing abundant quartz and glauconite (Fig. 16A). The carbonate fraction is subordinate and represented by small fragments of bivalves and echinoids interspersed in the more abundant siliciclastic component and lower in abundance with respect to the underlying deposits. The b/s ratio ranges between 0.002 and 0.4 whereas the S.I. indicates no segregation between bioclastic and siliciclastic particles. Locally, thin lenses of small rhodoliths occur, aligned along planar, sub-horizontal laminae (Fig. 16B). Burrowing is represented by *Thalassinoides* and *Skolithos* traces (Fig. 16C).

Depositional architectures.

Overall, *Facies 3b* appears to have no obvious internal sedimentary structures in close-up view but, in places, 20 to 30 cm thick angular foresets are visible, as well as intervals with plane-parallel lamination with similar thicknesses (Fig. 16A). At larger scale, these deposits exhibit an indistinct low-angle stratification, with individual strata 40 cm thick on average, pinching-out eastward, in the same direction of the ridge elongation (i.e. axis).

Interpretation.

The deposits of Facies Association 3 record the final abandonment of the Bombile tidal sand ridge after a period of intense activity and accretion. The deactivation of the ridge might have occurred at the end of a lowstand stage, during which time the sea-level stillstand in such an uplifting setting corresponds with the lowest relative sea level. During this stage, shallow-marine physical processes intersected the topographic profile of the active ridge. Consequently, the abrasion generated by energetic surface waves is a first process candidate for the genesis of the erosional surface that separates the cross-stratified deposits from the overlying planar deposits of *Facies 3a*. An alternative hypothesis is that erosion may have occurred after the passage of repeated trains of internal waves, which are common along surfaces separating stratified water masses with diverse density and temperature. Considering the inferred depth of the tidal sand ridge, and that such a condition is common today in the central Mediterranean, this seems to be the more realistic interpretation.

Sediments of *Facies 3b* overlie the previous deposits without any relevant erosion and represent the type of sedimentation that commonly seals a moribund tidal sand ridge and records the final stage of abandonment (e.g. Kenyon *et al.*, 1981). Siliciclastic sands may have been derived from the reworking of the underlying deposits by currents or surface waves in a general lower shoreface-offshore transition environment or deeper (e.g. Berné *et al.*, 2002). Such a relatively shallow-marine setting may explain the presence of rhodoliths.

DISCUSSION

Tidal sand ridges in the Siderno Strait: do they match existing models?

The deposits documented in this study point to nucleation, accretion and abandonment of an individual mixed bioclastic-siliciclastic tidal sand ridge (Table 1). This very large-scale subaqueous bedform developed (together with other parallel ridges in the same basinal sector) with the onset of vigorous tidal currents in the Siderno Strait during the Early Pleistocene (see Figs 1A and 2A).

Many of the attributes documented for modern and ancient tidal sand ridges, in both

Table 1. Summary of the facies and facies associations and their quantitative features recognized in the studied succession, with included the suggested genetic processes and the correspondent stages of nucleation, active accretion and abandonment of the tidal sand ridge of Bombile

Facies associations	Facies description	Average bed thickness (m)	Bioclastic/siliciclastic ratio (b/s)	Segregation Index (S.I.)	Bioturbation Index (B.I.)	Ichnofacies
			(Chiarella & Longhitano, 2012)	Taylor & Goldring (1993)	Fossils	Minter et al. (2016)
Facies association 3	Facies 3b = Structureless or indistinctly cross-stratified texturally mature sands	–	<<1 (0.002–0.4)	Unsegregated (30–35)	Uncommon to Moderate (2–3)	<i>Thalassinoides</i> , <i>Skolithos</i>
Facies Association 2	Facies 3a = highly burrowed, planar-stratified and internally laminated biocalcarenites, lapping against the s2 erosional surface	0.2–0.4	1 to >>1 (0.8–4.0)	Unsegregated (30–35)	Common (4)	<i>Thalassinoides</i> , <i>Skolithos</i> , <i>Bichordites</i> (Caruso et al., 2011)
Facies Association 2	Facies 2d = planar-stratified, fine-grained biocalcarenites, highly-bioturbated and containing no cross-strata (Fig. 12)	0.5–1.0	>>1 (4.0–9.09)	Poorly segregated (40–50)	Common to abundant (4–5)	Planktonic: <i>Globigerinoides ruber</i> , <i>Orbulina universa</i> , <i>Globigerina bulloides</i> ; Benthonic: <i>Orbitoides</i> (Fig. 15D)
Facies Association 2	Facies 2c = highly-bioturbated fine-grained bioclastic–siliciclastic sandstone intercalations. Fe–Mn nodules and glauconite (Fig. 11)	1.0–1.5	>1 to =1 (1.0–1.5)	Unsegregated (30–35)	Moderate (3)	Planktonic: <i>Globigerina bulloides</i> ; Benthonic: <i>Orbitoides</i> (Fig. 12E)
Facies Association 2	Facies 2b = large-scale trough-x-stratified bioclastic–siliciclastic sandstones, including angular to tangential, simple and compound foresets, tidal bundles, localized herringbone cross-stratification and reactivation surfaces (Figs 8, 9 and 10)	5.0–7.0	1 to >>1 (0.7–7.0)	Moderately to well segregated (60–85)	Moderate to common (3–4)	Planktonic: <i>Globigerinoides ruber</i> , <i>Orbulina universa</i> , <i>O. suturalis</i> , <i>Globigerina bulloides</i> ; Benthonic: <i>Orbitoides</i> (Fig. 8E)

siliciclastic-dominated and carbonate-dominated case studies (Houbolt, 1968; Pryor *et al.*, 1990; Davis & Balson, 1992; Keith & Zuppann, 1993; Hulscher, 1996; Saito *et al.*, 1998; Reynaud *et al.*, 1999; Berné *et al.*, 2002; Park *et al.*, 2006; Reeder & Rankey, 2008; Chiarella *et al.*, 2020) resemble the characteristics observed in the studied succession of the Siderno Basin. Particularly, superimposed dunes migrating obliquely with respect to the ridge axis and the tripartite facies association recording nucleation, accretion and abandonment of the ridge are common distinctive elements of these systems (Caston, 1972, 1981; McCave & Langhorne, 1982; Huthnance, 1982a; Huthnance, 1982b; Howarth & Huthnance, 1984; Gaynor & Swift, 1988). The present-day Celtic Sea (Fig. 17A) provides a possible modern analogue for a depositional setting similar to that envisaged for the Siderno Strait (Fig. 17B). South-west of the conjunction between the Irish Channel and the English Channel, linear tidal sand ridges developed during the Holocene to a depth coinciding with the shelf edge. In the Bombile deposits, physical attributes common to this modern example include: (i) orientation of the ridge axis approximately parallel to the expected basin-scale sediment transport pathway (Fig. 17A and B); (ii) large-scale progradational pattern generated during the early and mature stage of ridge accretion (Fig. 18); (iii) occurrence of large-scale trough cross-strata with the direction of advancement oriented at high angle with respect to the axis of elongation of the ridge; and (iv) tripartite subdivision of nucleation, maturity and abandonment stages expressed by the two facies associations (FA2 to FA3; Fig. 18).

However, there are also some notable differences. Most of the shelf-ridge examples referenced above have been interpreted as transgressive features (Fig. 17A), reworking older lowstand deposits, with only a few of them referred to as 'regressive'. The facies-based documentation herein suggests that the Bombile sand ridge represents a regressive tidal sand ridge, that started accreting during a period of slow fall of relative sea-level (highstand + tectonic uplift) and actively migrated during a subsequent stage of more severe relative sea-level drop (fall and lowstand + tectonic uplift). Moreover, the Bombile ridge deposits have a mixed bioclastic-siliciclastic composition. This characteristic is an important difference from the reference models, especially in the absence of other documented examples of 'mixed' tidal ridges in the literature. The Bombile sand ridge was in

fact dominantly supplied from autochthonous and parautochthonous carbonate factories, and only subordinately from clastic terrigenous detritus, as indicated for many reference models (e.g. Leva López *et al.*, 2016; Michaud & Dalrymple, 2016).

Although the Bahama Banks represent an example of pure carbonate sand ridges, they differ from the present case study because of their shallower depth. Moreover, the Bahamas modern example is fed by a carbonate photozoan association, developed in tropical settings, whereas the Pleistocene Bombile example was supplied from the bioclastic product of a carbonate heterozoan association, developed in a deeper temperate setting. Finally, the effect of siliciclastic input on the factory distribution and production, and its variation in terms of budget during the relative sea-level changes can play a significant role (Chiarella *et al.*, 2019).

Genesis of the mixed tidal ridge in the Siderno Basin

During the early Pleistocene, the narrow, linear basins dissecting the Calabrian Arc and connecting the Tyrrhenian with the Ionian Sea (see Fig. 1B) were subject to a major episode of structural narrowing (Ghisetti, 1979; Monaco & Tortorici, 2000; Rossetti *et al.*, 2001). Weak currents flowing through these corridors were at first associated with conditions of non-tidal strait. As the restricting marine corridors reached their 'critical cross-section' (i.e. a cross-section of the strait whose dimension is proportional to the mass of water flowing through it, leading to phenomena of hydraulic amplification; cf. Longhitano *et al.*, 2014), vigorous bi-directional currents established conditions for tide-dominated sedimentation. The Siderno Strait was one of the major tectonically controlled corridors in this setting, existing contemporaneously with the Catanzaro and Messina straits (Chiarella *et al.*, 2012; Longhitano *et al.*, 2012b). These basins are thought to have been characterized by a state of general sediment starvation, as the terrigenous inputs were limited to localized fan deltas and subaqueous erosion of bare substrate units (Rossi *et al.*, 2017). However, the onset of more energetic hydrodynamic conditions due to tidal amplification promoted additional clastic sources provided by carbonate skeletal grains coming from organisms populating hard and mobile substrates (Colella & D'alessandro, 1988). In the Messina and

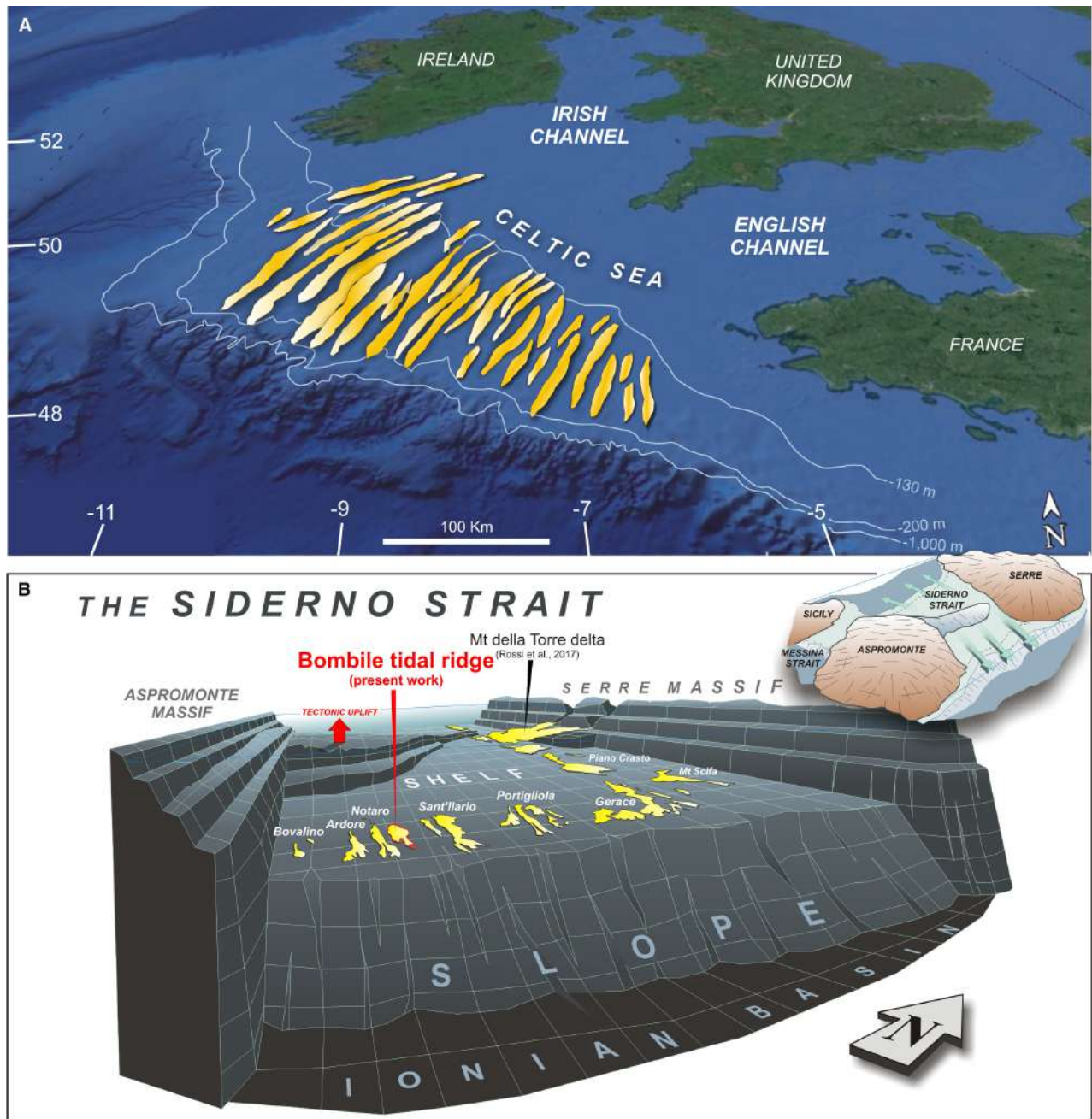


Fig. 17. (A) Modern comparative analogue for the Bombile sand ridge from the shelf area of the Celtic Sea, at the exit of the Irish and English Channels (satellite images is from Google Earth®; ridge reconstruction are from Scourse *et al.*, 2009). (B) Palaeogeographic reconstruction of the Siderno Strait, as seen from the south-east, during the accretion of tidal sand ridges, with the main sand bodies presently exposed in outcrops and the studied Bombile from the Pleistocene. The inset in the top-right corner shows the reconstruction of the Siderno Basin setting during the Pleistocene.

Catanzaro palaeostraits, these sediment sources resulted in the accumulation of mixed siliclastic/bioclastic deposits which were shaped by bidirectional to strongly asymmetrical currents

driven by tidal forcing into discontinuous dune fields (Chiarella *et al.*, 2012, 2016; Longhitano *et al.*, 2012b). In the case of Siderno Strait, tidal dunes converged along linear depositional

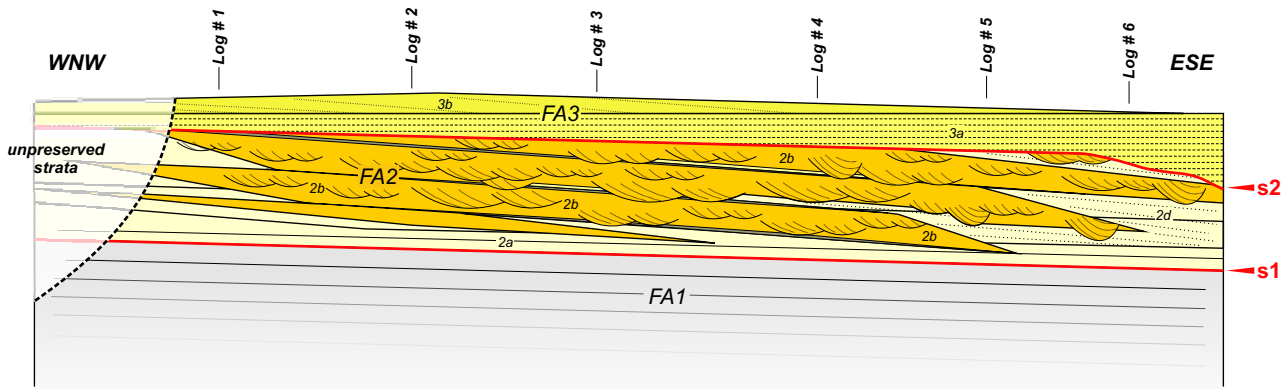


Fig. 18. Reconstructed schematic facies panel obtained for the investigated succession. The three facies associations (FA) correspond with the three main stages of ridge nucleation (FA1), active accretion (FA2) and abandonment (FA3).

bands, which developed into tidal ridges (Figs 17, 18 and 19A to C).

BIRTH, LIFE AND DEMISE OF THE BOMBILE TIDAL SAND RIDGE

The stratigraphic succession exposed in the Bombile Section records the birth, life and demise of an individual tidal sand ridge (Fig. 19A to C) suggesting that its evolution occurred during a complete cycle of relative sea-level change (Fig. 20). In particular, the architectures and facies assemblages (FA2 to FA3) documented here allow to unravel the development history of such a ridge, providing important insights on the oceanographic changes that affected the Siderno Basin and this sector of the central Mediterranean during the Early Pleistocene.

Environmental implications of the facies assemblage

Prior to the onset of a tide-dominated circulation, the Siderno Strait hosted the equivalent of open-shelf marine conditions. This stage is recorded in the fine-grained deposits of *Facies 1a* and *1b* and whose accumulation was mainly due to suspension fall-out and decelerating density currents (c.f. Talling *et al.*, 2012; Fig. 20) promoted by an oceanographic, non-tidal circulation deriving from water mass exchanges already occurring between adjacent basins (Longhitano *et al.*, 2012a).

The overlying bioclastic-rich deposits of facies association 2 (Fig. 18) indicate a sudden increase in oceanographic current strength. Low-angle cross-stratification of *Facies 2a* and the downlapping stratal terminations eroding slightly onto the underlying shelf deposits of FA2 (Fig. 18) suggest similarities with the large-scale lateral accretion features described for modern offshore tidal sand banks (e.g. Terwindt, 1971; Lapierre *et al.*, 1975; Yang, 1989) or interpreted from outcrop analogues (e.g. Houthuys & Gullentrops, 1988; Leva López *et al.*, 2016). These deposits, which form elongated progradational sand bodies FA2 (Figs 18 and 19A), suggest the nucleation of an initial tidal sand bank that formed the core of the forthcoming tidal sand ridge in this eastern side of the Siderno Basin (Fig. 17). As the tidal currents increased in strength, possibly due to the achievement of a tectonically-driven critical basinal cross-section promoting tidal amplification, large-scale sinuous-crested dunes of *Facies 2b* developed (Fig. 18). These dunes, which were dominantly composed of bioclasts and, subordinately, of siliciclasts derived from the erosion of older units exposed in adjacent subaqueous areas, started migrating to the south/south-east, advancing obliquely with respect to the ridge main axis (Fig. 19B). At a stage of maturity, the ridge accreted following rhythmic phases of advancement towards the east/south-east, which are recorded in the overall shingle architecture and marked by temporary pauses represented by the fine-grained intercalations of *Facies 2c* (see similar features described by Saha *et al.*, 2016). These horizons

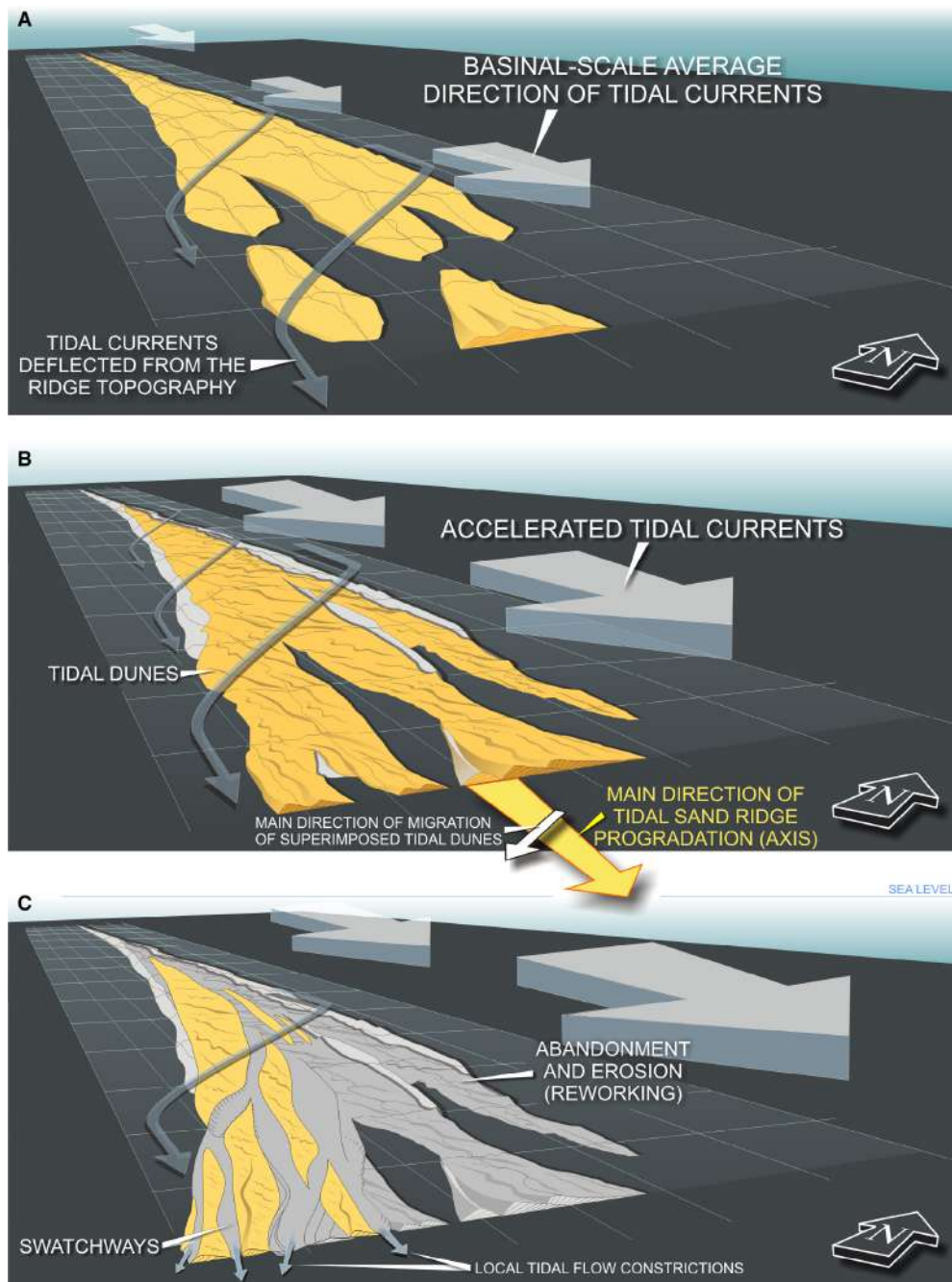


Fig. 19. Three-dimensional reconstruction of the stage of nucleation (A) and active accretion, (B) to (C) of the tidal sand ridge studied in the Bombile Section. The parts of the ridge in yellow indicate the most actively accreting portions during each stage. (A) At the initial stage of ridge nucleation, tidal currents were not yet able to promote the migration of large dunes because of their relatively low speeds. However, currents interacted with the bottom topography flowing at *ca* 20° with respect to the ridge axis. (B) As water-depth variations changed the cross-sectional area of the Siderno Strait, current speeds increased, promoting a more vigorous tidal circulation, the concomitant activation of the carbonate factory and the resulting generation of large (mostly three-dimensional) dunes, recording the fastest stage of active ridge accretion. Note the angular relationship between the direction of ridge axial progradation and the main direction of tidal dune migration. (C) As the sea level reached its lowermost elevation (LST), dunes were dissected by swatchways, reflecting the highest stage of current regime, prior to the ensuing deactivation due to transgression. Drawing not to scale.

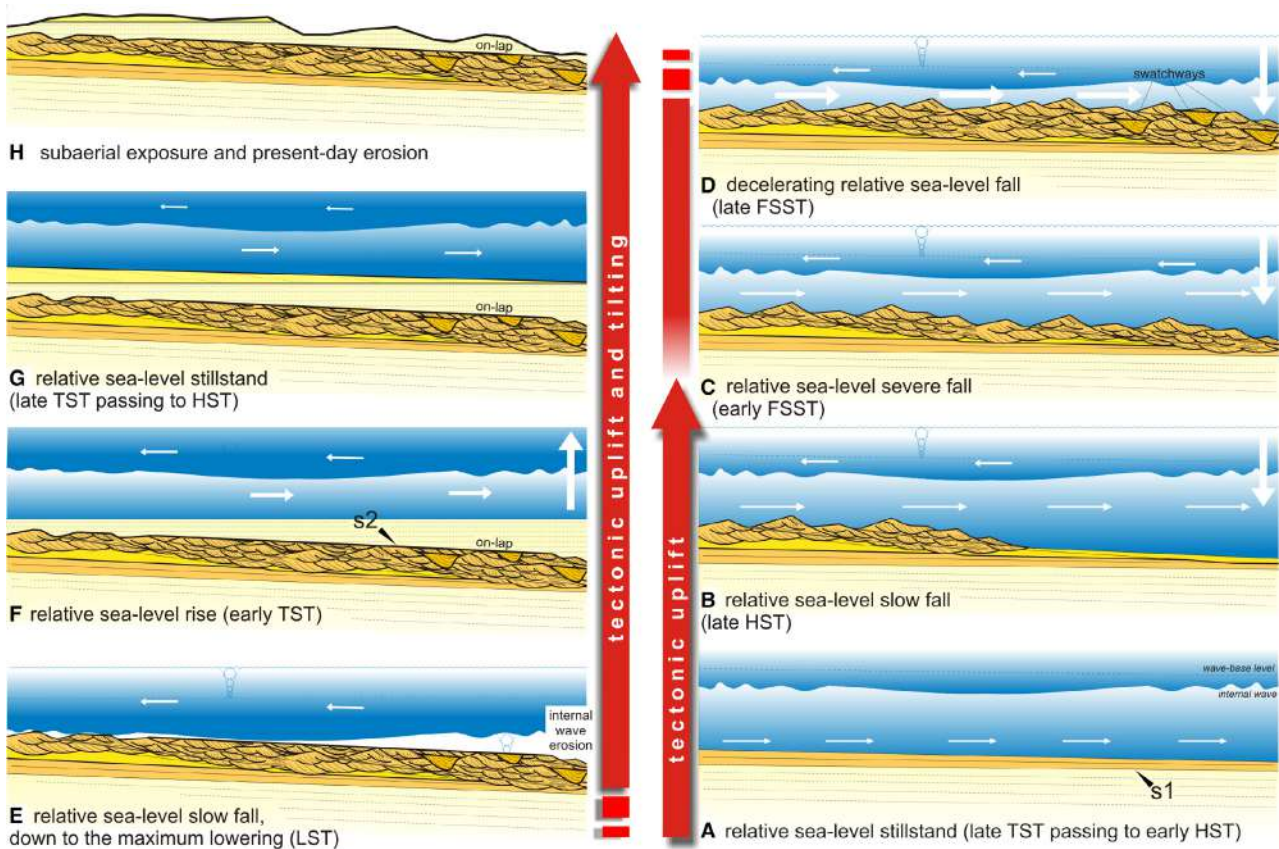


Fig. 20. Evolutionary panel showing the processes responsible for the accretion of the Bombile tidal sand ridge (see the text for explanation). Concerning the origin of the s2 discontinuity that separates the large-scale cross-strata from the overlying plane-parallel strata, it is attributed to the role of internal waves generated at the boundary between two superimposed water masses with different density.

represent ‘accretion surfaces’ (cf. Leva López *et al.*, 2016), over which the ridge migrated after a stage of abandonment. During their energetic stages of migration, tidal dunes also exhibited isolated sectors with low-energy conditions. Such inter-dune areas or swales lateral to the main sediment transport routes (Fig. 19B and C), hosted fine-grained mixed sands of *Facies 2d*, providing favourable conditions for proliferation of infaunal organisms (c.f. MacEachern *et al.*, 2007).

The sub-horizontal stratification of the topmost interval in the Bombile ridge (FA3) records another important oceanographic change in the Siderno Strait and, presumably, the restoring of conditions of hemipelagic sedimentation in moderate energy after a phase of tidal dominance. This episode also corresponds with the abandonment of the ridge and the end of its active migration because of its ultimate burial (c.f. Yang, 1989).

Relative sea-level changes as the main controlling factor in the tidal sand ridge evolution

The documented ridge succession shows physical attributes that may be related to at least two orders of relative sea-level change: (i) a major long-term cycle, spanning a few 100 kyr, which controlled the large-scale sand ridge architecture (i.e. initiation, progradation and abandonment); and (ii) a number of superimposed shorter-term minor cycles. These smaller sea-level oscillations were possibly driven by Milankovitch-scale orbital perturbations (<100 kyr) that are known to have controlled shelf sedimentation in the Siderno Basin during the Pliocene (Gudjonsson, 1987; Hilgen, 1987; De Visser *et al.*, 1989; Lourens *et al.*, 1992).

The long-term cycle is recorded by the three facies associations in the Bombile Section (Fig. 18).

The base of the tide-dominated portion of the ridge indicates erosion of the underlying shelf deposits and defines a descending basinward trajectory. This stratigraphic element could reflect a longer-term stage of relative sea-level lowering and reduced accommodation, imparted by the tectonic uplift of the central sill of the Siderno Basin (i.e. the Aspromonte Massif). This regional event was probably one of the major factors causing tidal amplification in the Siderno Basin, which in turn promoted the nucleation of early-stage juvenile tidal sand ridges (Figs 19A and 20A).

Large-scale tidal dunes, evidenced by complex cross-stratification in the Bombile Section, represent a major stage of ridge accretion and migration, reflecting a dynamic environment influenced by short-term relative sea-level oscillations that caused changes in the intensity of the currents (Fig. 19B). Trough cross-strata show 'ascending to descending' trajectories in lateral views (Fig. 10A to D), inferred to have been forced by high-frequency, low-amplitude changes in relative sea level, forcing the dunes to erode the underlying deposits during stages of sea-level lowering and aggrading during ensuing periods of sea-level rise (c.f. Longhitano & Nemeč, 2005).

During this stage, smaller bedforms superimposed on the top of larger dunes are common, indicating palaeocurrent directions oriented at high angle with respect to the dominant transport direction. This feature can be explained by the influence of the opposite (ebb) currents during stages of sea-level lowering, due to a general increase of tidal friction related to shallower conditions (Fig. 20B and C).

At the end of the phase of long-term relative sea-level fall, or at least during its latest stage, the minimum water depth probably enhanced the tidal power as a result of the extreme tidal flow constriction (e.g. Anastas *et al.*, 2006). The reduced depth also promoted the incision of inter-dune channels or swatchways, which eroded several metres into the underlying dunes (Fig. 20C). Swatchways occur in fact only in the basinward (eastward) portion of the Bombile Section that presumably records the latest stage of tidal sand ridge progradation at the end of relative sea-level fall. The development of several generations of swatchways, existing for a short time and actively migrating laterally, was possibly the main cause for the branching aspect of the outcrop in the present-day plan view (i.e. the easternmost portion of the Bombile Section), as well as in many of the other

ridges in the eastern side of the Siderno Basin. At this stage, the up-dip (north-west) portion of the ridge was possibly even less migratory, whereas the basinward continuation (south-east) advanced with higher rates, resulting in multiple minor ridges, as also observable in the adjacent correlative deposits of the Notaro and Ardore (Fig. 17) sections.

Lowstand deposits recording the latest stages of tidal dominance have not been detected in the Bombile Section, probably because of the poor preservation of the south-easternmost portion of the outcrop, or they are located farther out in deep-water areas. At the end of the falling of relative sea level the crests of the dunes were smoothed by erosion, generating the *s2* discontinuity visible at the top of the trough cross-bed complex (Fig. 20E). This sharp discontinuity marks an abrupt change that is thought to be related to bypass of sediments to areas of additional accommodation and a subsequent phase of relative sea-level rise, Fig. 20F).

The topmost *FA3* deposits record the final stage of cessation of ridge activity. Planar-stratified facies included in this association exhibit features indicating low sediment accumulation rates and sedimentation with no preserved tidal influence.

The lateral stratal terminations lapping against the back edge of the ridge and sealing the underlying large-scale cross-strata by onlap onto the *s2* discontinuity suggest that this stage of ridge burial occurred during a major phase of relative sea-level rise. This is similar to deposits in the adjacent Messina and Catanzaro straits, as these marine corridors widened due to transgression, they lost the critical conditions necessary for tidal amplification, transitioning from tide-dominated straits into non-tidal seaways (e.g. Chiarella *et al.*, 2012, 2014; Longhitano *et al.*, 2014; Longhitano, 2018b). The upward transition to siliciclastic-rich deposits at the very top of the section records deposition during a relative-sea-level highstand and the accumulation of prograding well-sorted shelf sands deriving from the reworking of the underlying strata (Fig. 20G).

Possible role of internal waves

The palaeo-depth of the investigated sector of the Siderno Basin during the development of the active tidal sand ridge can be estimated by using the proportions suggested by Snedden & Dalrymple (1999). These authors argue that

sand-ridge thickness corresponds at least to *ca* 20% of the water column depth at its active stage. An estimation of the primary tidal dune height is provided by the 'Kolmogorov ratio' (Kolmogorov, 1951). This relatively simple statistical application helps with evaluating deposition/erosion proportions of cross-stratified subtidal deposits (e.g. Longhitano & Nemec, 2005; Longhitano *et al.*, 2014; Longhitano, 2018b). For the present dataset, this ratio is $k = 0.05$ to 0.07 , indicating an overall post-depositional erosion of the dune tops of *ca* 5 to 7%. Since the cross-stratified interval has an average thickness of *ca* 50 m in its thickest central portion (Fig. 5), the maximum inferred water depth in this sector of the Siderno Basin was up to 270 m during the growth of the ridge. The rate of down-current migration is thought to have been high, as is typical in ocean areas subject to strong tidal asymmetry (e.g. Dalrymple & Hoogendoorn, 1997). However the ridge, at least in its north-western portion, still preserves its original nucleus (*Facies 2a*) indicating that an episode of rapid abandonment occurred prior to the stage of full ridge maturity (i.e. Class II of Snedden & Dalrymple, 1999).

The origin of the *s2* discontinuity that abruptly interrupts the spectacular sequence of trough cross-strata exposed in the Bombile Section (*Facies 2b*) is a little uncertain. Indeed, it seems to have been generated by a persistent process of subaqueous erosion of the underlying tidal dunes that produced, as a result, the flattening of a previously undulating bottom topography. It is worth noting that the responsible process appears to have acted at a semi-basinal scale, rather than at a local scale, because this surface is observable in all of the sections exposing this stratigraphic interval in the Siderno Basin. Based on the depth estimation, erosion produced by waves (i.e. wave ravinement) is not a reasonable process candidate to explain the origin of this discontinuity. The authors attribute this discontinuity to the repeated erosion produced by the passage of trains of internal waves (c.f. He & Gao, 1999; Pomar *et al.*, 2012; Fig. 20E). The present-day central Mediterranean waters flowing through the Messina Strait are strongly stratified, due to differences in salinity and density between two main flows: the northward-directed flux of the denser *Levantine Intermediate Water (LIW)* and the southward-directed and lighter *Tyrrhenian Surface Water (TSW)* (Alpers & Salusti, 1983; Brandt *et al.*, 1997). The superimposed currents exert unequal influences

on mobile sediments at the sea bottom (Longhitano, 2018a). Because the movement of these water masses is regulated by semi-diurnal tidal cyclicity and reversals, the tidal exchange between the two adjacent basins is superimposed on trains of bi-directional internal waves moving along the subaqueous interface that separates the two superimposed currents (Droghei *et al.*, 2016). In the modern Messina Strait, this interface occurs at an average depth of *ca* 100 m, and the internal waves that run along the pycnocline every semi-diurnal tidal cycle reach a peak velocity of *ca* 3 m s^{-1} when transiting across the narrowest, 3 km wide, strait centre. It is reasonable to infer that the same hydrodynamic setting occurred during the Early Pleistocene across the Calabrian corridors connecting the Tyrrhenian and Ionian seas, including the Siderno Basin. Considering a pycnocline at a depth of *ca* 100 m, as in the modern Messina Strait, the repeated passage of internal waves may have caused the erosion recorded by the *s2* discontinuity observed in the Bombile Section. Such waves, travelling with a velocity ranging between 0.5 m s^{-1} and 0.8 m s^{-1} (Droghei *et al.*, 2016), may have been capable of removing the unconsolidated bioclastic sands forming the crests of the highest dunes during the late stage of relative sea-level lowstand, exerting a diffuse basin-scale process of bottom flattening.

CONCLUSIONS

During the Early Pleistocene, the Siderno Strait was *ca* 20 km wide, connecting the Tyrrhenian and Ionian seas. In the Siderno Strait, currents moving westward (flood) and eastward (ebb) were amplified by the presence of a central, shallowly submerged Aspromonte tectonic high characterized by erosion or non-deposition. On both sides of this horst, a variety of bedforms developed, migrating outward from the strait centre. Here, the Lower Pleistocene sediments that record the strait opening and then closing are well-exposed. In particular, a series of tidal sand ridges with superimposed dunes developed close to the south-eastern end of the strait, where bathymetry was deeper and flow expansion occurred. Due to the positioning of the ridges with respect to the shelf edge and the strait-centre zone, the present-day Celtic Sea is a reasonable modern analogue for this case study, as linear tidal sand ridges developed south-west of the English Channel.

Three facies associations occur in the 120 m thick, siliciclastic–bioclastic succession of Bombile, distinguished by their sedimentological features, relative abundance of bioclastic and siliciclastic sediment fractions, and their depositional geometries. Facies Association 2 (FA2) and Facies Association 3 (FA3) record stages of nucleation, active accretion and abandonment, respectively, of an individual tidal sand ridge, possibly during a complete cycle of relative sea-level change. The lowermost interval of FA2 records the juvenile stage of the ridge, likely during high sea level. The intermediate portion of FA2, characterized by bioclastic-rich, large-scale trough cross-strata, developed from the SSE-migration of sinuous-crested tidal dunes, forming the core of the ridge. Cyclical aggrading to prograding foreset architectures, possibly forced by high-frequency sea-level changes, are interpreted in terms of a long-lasting phase of relative sea-level fall. Sea-level fall and tectonic uplift conditions appear to have enhanced the incision of channels or ‘swathways’ in the interdune troughs and the splitting of the ridge into multiple minor ridges, because of the strengthened tidal current energy. At the late stage of relative sea-level lowstand, trains of internal waves eroded the top of the ridge. The subsequent transgression deactivated the Bombile ridge, leading to a mantling of non-tidal bioclastic-rich fines of FA3. This suggests that less energetic conditions were present in the strait during relative sea-level rise, possibly because of expanded basin dimensions, and reduced tidal amplification.

During the stage of ridge active accretion (intermediate FA2), an *in situ* to *near situ* heterozoan carbonate factory supplied skeletal grains for the growth of the Bombile ridge through short-distance transport by strong active tidal currents. The reduced siliciclastic fraction input derives from the erosion of the Mesozoic–Cenozoic strata of the Aspromonte high, in a subaqueous setting with combined action of waves and currents.

The authors suggest that tidal sand ridges can also develop in confined subaqueous settings, such as straits, and not only in open-shelf settings. Key conditions seem to be: (i) current amplification and enhanced bed-shear stress, causing sufficient friction to transport and deposit sand-size sediment once currents decelerate; (ii) bathymetric shallowing, rather than only narrowing, necessary for providing diffuse current patterns rather than concentrated or converging flows; (iii) persistent currents that can allow the ridge to nucleate and

actively accrete; and (iv) in the case of deposits with mixed (bioclastic/siliciclastic) composition, as in the present study, specific environmental conditions necessary for allowing living organisms to populate the bedforms during the more active stage of ridge development.

ACKNOWLEDGEMENTS

We would like to thank the University of Basilicata, UT Austin, and GSA Research Grant (10724-14) for financial support to the field activities. We thank Cornel Olariu and Luis Pomar for very useful discussions, Angela Laviano for the assistance in microfossil identification, Vincenzo Tolla for thin-section lab. facilities, and Safari Project for LiDAR and drone acquisition. Our gratitude goes to Carlo Messina, Peter Flaig and a third anonymous reviewer, as well as to Associate Editor Anna Pontén, for their very insightful comments to the early version of this manuscript. DC thanks OKEA ASA for supporting the Clastic Sedimentology Investigation (CSI) group.

DATA AVAILABILITY STATEMENT

Research data are not shared.

REFERENCES

- Abreu, V.S. and Anderson, J.B. (1998) Glacial eustasy during the Cenozoic: sequence stratigraphic implications. *Am. Assoc. Petroleum Geol. Bull.*, **82**, 1385–1400.
- Allen, J.R.L. (1968) *Current Ripples: Their Relation to Patterns of Water and Sediment Motion*. Science, North-Holland, Amsterdam, 433 pp.
- Allen, J.R.L. (1980) Sand waves: a model of origin and internal structure. *Sediment. Geol.*, **26**, 281–328.
- Allen, J.R.L. (1982) *Sedimentary Structures: Their Character and Physical Basis*. Elsevier, Amsterdam, 539 pp.
- Allen, P.A. and Homewood, P. (1984) Evolution and mechanics of a Miocene tidal sandwave. *Sedimentology*, **31**, 63–81.
- Alpers, W. and Salusti, E. (1983) Scylla and Charybdis observed from space. *J. Geophys. Res.*, **88**, 1800–1808.
- Amodio-Morelli, L., Bonardi, G., Colonna, V., Dietrich, D., Giunta, G., Ippolito, F., Liguori, V., Lorenzoni, S., Paglionico, A., Perrone, V., Piccarreta, G., Russo, M., Scandone, P., Zanettin Lorenzoni, E. and Zuppetta, A. (1976) L’arco Calabro-Peloritano nell’orogene Appenninico-Maghrebide. *Memorie della Società Geologica Italiana*, **17**, 1–60.
- Anastas, A.S., Dalrymple, R.W., James, N.P. and Nelson, C.S. (1997) Cross-stratified calcarenites from New Zealand: subaqueous dunes in a cool-water, Oligo-Miocene seaway. *Sedimentology*, **44**, 869–891.

- Anastas, A.S., Dalrymple, R.W., James, N.P. and Nelson, C.S. (2006) Lithofacies and dynamics of a cool-water carbonate seaway; mid-Tertiary, Te Kuiti Group, New Zealand. In: *Cool-Water Carbonates: Depositional Systems and Palaeoenvironmental Controls* (Eds Pedley, H.M. and Carranante, G.), vol. 255, pp. 245–268. Geological Society of London, London, UK.
- Androsov, A.A., Kagan, B.A., Romanenkov, D.A. and Voltzinger, N.E. (2002) Numerical modelling of barotropic tidal dynamics in the strait of Messina. *Adv. Water Resour.*, **25**, 401–415.
- Arnott, R.W. and Southard, J.B. (1990) Exploratory flow-duct experiments on combined-flow bed configurations, and some implications for interpreting storm-event stratification. *J. Sediment. Res.*, **60**, 211–219.
- Bádenas, B. and Aurell, M. (2001) Proximal-distal facies relationships and sedimentary processes in a storm dominated carbonate ramp (Kimmeridgian, northwest of the Iberian Ranges, Spain). *Sediment. Geol.*, **139**, 319–340.
- Bargagli, A. and Sannino, G. (2012) Modello di circolazione dello stretto di Messina. ENEA, Agenzia nazionale per le nuove tecnologie, l'energia e lo sviluppo economico sostenibile, Report Rds/2012/171, 22 p.
- Barrier, P. (1986) Évolution paléogéographique du Déroit de Messine au Pliocène et au Pléistocène. *Giorn Geol.*, **48**, 7–24.
- Barrier, P. (1987) Stratigraphie des dépôts pliocènes et quaternaires du Déroit de Messine. *Documents et Travaux, IGAL*, **11**, 59–81.
- Basso, D. (1998) Deep rhodolith distribution in the Pontian Islands, Italy: a model for the paleoecology of a temperate sea. *Palaeogeogr. Palaeoclimatol. Palaeoecol.*, **137**, 173–187.
- Belderson, R. (1986) Offshore tidal and non-tidal sand ridges and sheets: differences in morphology and hydrodynamic setting.
- Belderson, R.H., Johnson, M.A. and Kenyon, N.H. (1982) Bedforms. In: *Offshore Tidal Sands* (Ed. Stride, A.H.), pp. 27–57. Chapman and Hall, London.
- Belderson, R.H. and Stride, A.H. (1966) Tidal current fashioning of a basal bed. *Mar. Geol.*, **4**, 237–257.
- Berné, S., Vagner, P., Guichard, F., Lericolais, G., Liu, Z., Trentesaux, A., Yin, P. and Yi, H.I. (2002) Pleistocene forced regressions and tidal sand ridges in the East China Sea. *Mar. Geol.*, **188**, 293–315.
- Bonardi, G., Cavazza, W., Perrone, V. and Rossi, S. (2001) Calabria-Peloritani terrane and northern Ionian Sea. In: *Anatomy of an Orogen: The Apennines and Adjacent Mediterranean Basins* (Eds Vai, G.B. and Martini, I.P.), pp. 287–306. Springer Netherlands, Dordrecht.
- Bonardi, G., Giunta, G., Perrone, V., Russo, M. and Zuppetta, A.C.G. (1980) Osservazioni sull'evoluzione miocenica dell'Arco Calabro-Peloritano nel Miocene Inferiore: la Formazione di Stilo-Capo d'Orlando.
- Bonardi, G., Messina, A., Perrone, V. and Russo, S. (1984) L'Unità di Stilo nel settore meridionale dell'Arco Calabro-Peloritano.
- Braga, J.C., Martín, J.M., Aguirre, J., Baird, C.D., Grunnaleite, I., Jensen, N.B., Puga-Bernabéu, A., Sælen, G. and Talbot, M.R. (2010) Middle-Miocene (Serravallian) temperate carbonates in a seaway connecting the Atlantic Ocean and the Mediterranean Sea (North Betic Strait, S Spain). *Sediment. Geol.*, **225**, 19–33.
- Brandt, P., Rubino, A., Alpers, W. and Backhaus, J.O. (1997) Internal waves in the Strait of Messina studied by a numerical model and synthetic aperture radar images from the ERS 1/2 satellites. *J. Phys. Oceanogr.*, **27**, 648–663.
- Brandt, P., Rubino, A., Quadfasel, D., Alpers, W., Sellschopp, J. and Fiekas, H.-V. (1999) Evidence for the influence of atlantic-ionian stream fluctuations on the tidally induced internal dynamics in the strait of Messina. *J. Phys. Oceanogr.*, **29**, 1071–1080.
- Canals, M. and Ballesteros, E. (1997) Production of carbonate particles by phytobenthic communities on the Mallorca-Menorca shelf, northwestern Mediterranean Sea. *Deep Sea Res. Part II Top. Stud. Oceanogr.*, **44**, 611–629.
- Carminati, E., Lustrino, M. and Doglioni, C. (2012) Geodynamic evolution of the central and western Mediterranean: tectonics vs. igneous petrology constraints. *Tectonophysics*, **579**, 173–192.
- Caruso, C., Sonnino, M. and Uchman, A. (2011) Trace fossils in the Pleistocene arenites outcropping nearby the village of Bombile (southern Ionian Calabria). *Rendiconti Online SGI*, **17**, 59–61.
- Caston, G.F. (1981) Potential gain and loss of sand by some sand banks within Southern Bight of the North Sea. *Mar. Geol.*, **41**, 239–250.
- Caston, V.N.D. (1972) Linear sand banks in the Southern North Sea. *Sedimentology*, **18**(63), 63–78.
- Cavazza, W., Blenkinsop, J., de Celles, P.G., Patterson, R.T. and Reinhardt, E.G. (1997) Stratigrafia e sedimentologia della sequenza sedimentaria oligocenica-quaternaria del bacino calabro-ionico. *Bollet. Soc. Geol. Ital.*, **116**, 51–77.
- Cavazza, W. and DeCelles, P.G. (1993) Geometry of a Miocene submarine canyon and associated sedimentary facies in southeastern Calabria, southern Italy. *Geol. Soc. Am. Bull.*, **105**, 1297–1309.
- Cavazza, W. and Ingersoll, R.V. (2005) Detrital modes of the Ionian Forearc basin fill (Oligocene-Quaternary) reflect the tectonic evolution of the Calabria-Peloritani Terrane (Southern Italy). *J. Sediment. Res.*, **75**, 268–279.
- Chiarella, D. (2016) Angular and tangential toset geometry in tidal cross strata: an additional feature of current-modulated deposits. In *Contributions to Modern and Ancient Tidal Sedimentology: Proceedings of the Tidalites 2012 Conference* (Eds Tessier, B. and Reynaud, J.-Y.), pp. 185–195. IAS Special Publication, Hoboken, NJ.
- Chiarella, D. and Longhitano, S.G. (2012) Distinguishing depositional environments in shallow-water mixed, bi-siliciclastic deposits on the basis of the degree of heterolithic segregation (Gelasian, Southern Italy). *J. Sediment. Res.*, **82**, 969–990.
- Chiarella, D., Longhitano, S.G. and Muto, F. (2012) Sedimentary features of the Lower Pleistocene mixed siliciclastic-bioclastic tidal deposits of the Catanzaro Strait (Calabrian Arc, south Italy). *Rend. Online Soc. Geol. Italy*, **21**, 919–920.
- Chiarella, D., Longhitano, S.G. and Tropeano, M. (2017) Types of mixing and heterogeneities in siliciclastic-carbonate sediments. *Mar. Petroleum Geol.*, **88**, 617–627.
- Chiarella, D., Longhitano, S.G. and Tropeano, M. (2019) Different stacking patterns along an active fold-and-thrust belt—Acerenza Bay, Southern Apennines (Italy). *Geology*, **47**, 139–142.
- Chiarella, D., Longhitano, S.G., Mosdell, W. and Telesca, D. (2020) Sedimentology and facies analysis of ancient sand ridges: Jurassic Rogn Formation, Trøndelag Platform, offshore Norway. *Mar. Pet. Geol.*, **112**, 104082.
- Chiarella, D., Moretti, M., Longhitano, S.G. and Muto, F. (2016) Deformed cross-stratified deposits in the Early Pleistocene tidally-dominated Catanzaro strait-fill

- succession, Calabrian Arc (Southern Italy): triggering mechanisms and environmental significance. *Sediment. Geol.*, **344**, 277–289.
- Colella, A.** (1996) I depositi dello Stretto di Messina, un'area ad elevata instabilità ambientale. In: *Excursion Guide Book of the Gruppo di Sedimentologia del CNR* (Ed. Colella, C.), *Annual Meeting, 10–14 October, Catania*, pp. 7–20.
- Colella, A.** and **D'alessandro, A.** (1988) Sand waves, Echinocardium traces and their bathyal depositional setting (Monte Torre Palaeo Strait, Plio-Pleistocene, southern Italy). *Sedimentology*, **35**, 219–237.
- Critelli, S., Putignano, M.L., Minzoni, N., Muto, F., di Stefano, A., Maniscalco, R., Cirrincione, L., Ortolano, G., Russo, R., Tripodi, V. and Vincenzi, S.** (2015) *Carta Geologica in scala 1:50.000 del Foglio n. 603 'Bovalino'*. Progetto C.A.R.G., I.S.P.R.A.
- Cucco, A., Quattrocchi, G., Olita, A., Fazioli, L., Ribotti, A., Sinerchia, M., Tedesco, C. and Sorgente, R.** (2016) Hydrodynamic modelling of coastal seas: the role of tidal dynamics in the Messina Strait, Western Mediterranean Sea. *Nat. Hazards Earth Syst. Sci.*, **16**, 1553–1569.
- Dalrymple, R.W.** (1980) Surge marks: are they water-escape structures? *Sedimentology*, **27**, 341–343.
- Dalrymple, R.W.** (2010) Tidal depositional systems. In: *Facies Models 4* (Eds James, N.P. and Dalrymple, R.W.), vol. **4**, pp. 201–231. Geological Association of Canada.
- Dalrymple, R.W.** and **Hoogendoorn, E.L.** (1997) Erosion and deposition on migrating shoreface-attached Ridges, Sable Island, Eastern Canada. *Geosci. Can.*, **24**(1), 25–36.
- Dalrymple, R.W.** and **Rhodes, R.N.** (1995) Estuarine dunes and bars. In: *Geomorphology and Sedimentology of Estuaries - Developments in Sedimentology* (Ed. Perillo, G.M.E.), Vol. **53**, pp. 359–422. Elsevier, Amsterdam.
- Davis, R.A.** and **Balson, P.S.** (1992) Stratigraphy of a north-sea tidal sand ridge. *J. Sediment. Petrol.*, **62**, 116–121.
- Davis, R.A., Klay, J. and Jewell, P.** (1993) Sedimentology and stratigraphy of tidal sand ridges Southwest Florida inner shelf. *J. Sediment. Res.*, **63**, 91–104.
- De Visser, J.P., Ebbing, J.H.J., Gudjonsson, L., Hilgen, F.J., Jorissen, F.J., Verhallen, P.J.J.M. and Zevenboom, D.** (1989) The origin of rhythmic bedding in the Pliocene Trubi Formation of Sicily, southern Italy. *Palaeogeogr. Palaeoclimatol. Palaeoecol.*, **69**, 45–66.
- Defant, A.** (1940) Scilla e Cariddi e le correnti di marea nello Stretto di Messina. *Geofisica Pura Applicata*, **2**, 93–112.
- Defant, A.** (1958) *Ebb and Flow: The Tides of Earth, Air and Water*. The University of Michigan Press, Ann Arbor.
- Desjardins, P.R., Buatois, L.A., Pratt, B.R. and Mángano, M.G.** (2012) Sedimentological-ichnological model for tide-dominated shelf sandbodies: Lower Cambrian Gog Group of western Canada. *Sedimentology*, **59**, 1452–1477.
- Dogliani, C.** (1991) A proposal for the kinematic modelling of W-dipping subductions - possible applications to the Tyrrhenian-Apennines system. *Terra Nova*, **3**, 423–434.
- Dogliani, C., Innocenti, F. and Mariotti, G.** (2001) Why Mt Etna? *Terra Nova*, **13**, 25–31.
- Dogliani, C., Merlini, S. and Cantarella, G.** (1999) Foredeep geometries at the front of the Apennines in the Ionian Sea (central Mediterranean). *Earth Planetary Sci. Lett.*, **168**, 243–254.
- Droghei, R., Falcini, F., Casalbore, D., Martorelli, E., Mosesti, R., Sannino, G., Santoleri, R. and Chiocci, F.L.** (2016) The role of Internal Solitary Waves on deep-water sedimentary processes: the case of up-slope migrating sediment waves off the Messina Strait. *Sci. Rep.*, **6**, 36376.
- Drooger, C.W. and Broekman, J.** (1973) *Messinian Events in the Mediterranean*, pp. 1–272. Elsevier Science & Technology, Amsterdam.
- Dumas, S., Arnott, R. and Southard, J.B.** (2005) Experiments on oscillatory-flow and combined-flow bed forms: implications for interpreting parts of the shallow-marine sedimentary record. *J. Sediment. Res.*, **75**, 501–513.
- Dyer, K.R. and Huntley, D.A.** (1999) The origin, classification and modelling of sand banks and ridges. *Cont. Shelf Res.*, **19**, 1285–1330.
- Gaynor, G.C. and Swift, D.J.P.** (1988) Shannon Sandstone depositional model; sand ridge dynamics on the Campanian Western Interior Shelf. *J. Sediment. Res.*, **58**, 868–880.
- Ghisetti, F.** (1979) Evoluzione neotettonica dei principali sistemi di faglie della Calabria centrale. *Bollet. Soc. Geol. Italiana*, **98**, 387–430.
- Ghisetti, F. and Vezzani, L.** (1982) Different styles of deformation in the calabrian arc (Southern Italy): Implications for a seismotectonic zoning. *Tectonophysics*, **85**, 149–165.
- Gorini, C., Montadert, L. and Haq, B.** (2019) Mediterranean Sea Level and Bathymetry of the Deep Basins During the Salt Giant Deposition: Inference from Seismic and Litho-Facies. In: *The Structural Geology Contribution to the Africa-Eurasia Geology: Basement and Reservoir Structure, Ore Mineralisation and Tectonic Modelling. CAJG (2018) Advances in Science, Technology & Innovation (IEREK Interdisciplinary Series for Sustainable Development)* (Eds Rossetti, F. et al.). Springer, Cham.
- Gudjonsson, L.** (1987) Local and global effects on the Early Pliocene Mediterranean stable isotope records. *Mar. Micropaleontol.*, **12**, 241–253.
- Harris, P.T., Pattiaratchi, C.B., Collins, M.B. and Dalrymple, R.W.** (1995) What is a bedload parting? In: *Tidal Signatures in Modern and Ancient Sediments* (Eds Flemming, B.W. and Bartholoma, A.), pp. 3–18. *International Association of Sedimentologists Special Publication 24*.
- He, Y.B. and Gao, Z.Z.** (1999) The characteristics and recognition of internal-tide and internal-wave deposits. *Chin Sci Bull.*, **44**, 582–589.
- Hilgen, F.J.** (1987) Sedimentary rhythms and high-resolution chronostratigraphic correlations in the Mediterranean Pliocene. *Stratigraphy Newsletter*, **17**, 109–127.
- Hilgen, F.J. and Langereis, C.G.** (1988) The age of the Miocene-Pliocene boundary in the Capo Rossello area (Sicily). *Earth Planetary Sci. Lett.*, **91**, 214–222.
- Hilgen, F.J. and Langereis, C.G.** (1993) A critical re-evaluation of the Miocene/Pliocene boundary as defined in the Mediterranean. *Earth Planetary Sci. Lett.*, **118**, 167–179.
- Houbolt, J.J.H.C.** (1968) Recent sediments in southern bight of the North Sea. *Geol. Mijnbouw*, **47**, 245–273.
- Houthuys, R. and Gullentrops, F.** (1988) Tidal transverse bars building up a longitudinal sand unit (Middle Eocene, Belgium). In: *Tide-Influenced Sedimentary Environments and Facies* (Eds de Boer, P.L., Nio, S.D. and Van Gelder, A.) pp. 153–166. Reidel, Dordrecht.
- Howarth, M.J. and Huthnance, J.M.** (1984) Tidal and residual currents around a Norfolk Sandbank. *Estuarine Coastal Shelf Sci.*, **19**, 105–117.
- Hulscher, S.J.M.H.** (1996) Tidal-induced large-scale regular bed form patterns in a three-dimensional shallow water model. *J. Geophys. Res.*, **101**, 20727–20744.

- Huthnance, J.M.** (1982a) On one mechanism forming linear sand banks. *Estuar. Coast. Shelf Sci.*, **14**, 79–99.
- Huthnance, J.M.** (1982b) On the formation of sand banks of finite extent. *Estuar. Coast. Shelf Sci.*, **15**, 277–299.
- James, N.P.** (1997) The cool-water carbonate depositional realm. In: *Cool-water Carbonates* (Eds. James, N.P. and Clarke, J.A.D.). *SEPM, v. Special Publications* **56**, 1–22.
- James, N.P., Seibel, M.J., Dalrymple, R.W., Besson, D. and Parize, O.** (2014) Warm-temperate, marine, carbonate sedimentation in an Early Miocene, tide-influenced, incised valley; Provence, south-east France. *Sedimentology*, **61**, 497–534.
- Keith, B.D. and Zuppann, C.W.** (1993) Mississippian oolites and petroleum reservoirs in the United States—an overview. In: *Mississippian Oolites and Modern Analogs* (Eds Keith, B.D. and Zuppann, C.W.), *AAPG Studies in Geology*, **35**, 1–12.
- Kenyon, N.H., Belderson, R.H., Stride, A.H. and Johnson, M.A.** (1981) Offshore tidal sand banks as indicators of net sand transport and as potential deposits. In: *Holocene Marine Sedimentation in the North Sea Basin* (Eds Nio, S.D., Shuttenehm, R.T.E. and van Weering, T.C.E.). *Int Assoc. Sedimentol., Spec. Publ.* **5**, 257–268.
- Knott, S.D. and Turco, E.** (1991) Late Cenozoic kinematics of the Calabrian Arc, southern Italy. *Tectonics*, **10**, 1164–1172.
- Kolmogorov, A.N.** (1951) Solution of a problem in probability theory connected with the problem of the mechanism of stratification. *Trans. Am. Math. Soc.*, **53**, 171–177.
- Lapierre, F., Boillot, G., Dunham, K.C. and Smith, A.J.** (1975) Contribution à l'étude géologique et sédimentologique de la Manche orientale. *Philos. Trans. R. Soc. Lond. A Math. Phys. Sci.*, **279**, 177–187.
- Leszczyński, S. and Nemeč, W.** (2020) Sedimentation in a synclinal shallow-marine embayment: Coniacian of the North Sudetic Synclinorium, SW Poland. *Depos. Rec.*, **6**, 144–171.
- Leva López, J., Rossi, V.M., Olariu, C. and Steel, R.J.** (2016) Architecture and recognition criteria of ancient shelf ridges; an example from Campanian Almond Formation in Hanna Basin, USA. *Sedimentology*, **63**(6), 1651–1676.
- Longhitano, S.G.** (2011) The record of tidal cycles in mixed silici-bioclastic deposits: examples from small Plio-Pleistocene peripheral basins of the microtidal Central Mediterranean Sea. *Sedimentology*, **58**, 691–719.
- Longhitano, S.G.** (2012) Microtidal straits: outcrop analogues from Calabria, south Italy. *Rendiconti Online della Società Geologica Italiana*, **21**, 937–939.
- Longhitano, S.G.** (2013) A facies-based depositional model for ancient and modern, tectonically-confined tidal straits. *Terra Nova*, **25**, 446–452.
- Longhitano, S.G.** (2018a) Between Scylla and Charybdis (part 1): the sedimentary dynamics of the modern Messina Strait (central Mediterranean) as analogue to interpret the past. *Earth-Sci. Rev.*, **185**, 259–287.
- Longhitano, S.G.** (2018b) Between Scylla and Charybdis (part 2): the sedimentary dynamics of the ancient, Early Pleistocene Messina Strait (central Mediterranean) based on its modern analogue. *Earth-Sci. Rev.*, **179**, 248–286.
- Longhitano, S.G., Chiarella, D., Di Stefano, A., Messina, C., Sabato, L. and Tropeano, M.** (2012b) Tidal signatures in Neogene to Quaternary mixed deposits of southern Italy straits and bays. *Sediment. Geol.*, **279**, 74–96.
- Longhitano, S.G., Chiarella, D. and Muto, F.** (2014) Three-dimensional to two-dimensional cross-strata transition in the lower Pleistocene Catanzaro tidal strait transgressive succession (southern Italy). *Sedimentology*, **61**, 2136–2171.
- Longhitano, S.G. and Chiarella, D.** (2020) Basic criteria for recognizing ancient tidal straits from the rock record. In: *Regional Geology and Tectonics* (Eds Scarselli, N., Adam, J. and Chiarella, D.). Elsevier, Amsterdam, Netherlands.
- Longhitano, S.G., Mellere, D., Steel, R.J. and Ainsworth, R.B.** (2012a) Tidal depositional systems in the rock record: a review and new insights. *Sediment. Geol.*, **279**, 2–22.
- Longhitano, S.G. and Nemeč, W.** (2005) Statistical analysis of bed-thickness variation in a Tortonian succession of biocalcarenic tidal dunes, Amantea Basin, Calabria, southern Italy. *Sediment. Geol.*, **179**, 195–224.
- Longhitano, S.G., Rossi, V.M., Chiarella, D., Mellere, D., Muto, F. and Tripodi, V.** (2021) From marginal to axial tidal-strait facies in the early Pleistocene Siderno Strait Tidalites Field Trips Special Volume Tidalites 2021, Matera, 2-4 October 2021, Field Trip T5. Geological Field Trips and Maps.
- Lourens, L.J., Hilgen, F.J., Gudjonsson, L. and Zachariasse, W.J.** (1992) Late Pliocene to early Pleistocene astronomically forced sea surface productivity and temperature variations in the Mediterranean. *Mar. Micropaleontol.*, **19**, 49–78.
- MacEachern, J.A., Pemberton, S.G., Gingras, M.K. and Bann, K.L.** (2007) CHAPTER 4 - The ichnofacies paradigm: a fifty-year retrospective. In: *Trace Fossils* (Ed. Miller, W.), pp. 52–77. Elsevier, Amsterdam.
- Madof, A.S., Bertoni, C. and Lofi, J.** (2019) Discovery of vast fluvial deposits provides evidence for drawdown during the late Miocene Messinian salinity crisis. *Geology*, **47**, 171–174.
- Malinverno, A. and Ryan, W.B.F.** (1986) Extension in the Tyrrhenian Sea and shortening in the Apennines as result of arc migration driven by sinking of the lithosphere. *Tectonics*, **5**, 227–245.
- Manzi, V., Gennari, R., Hilgen, F., Krijgsman, W., Lugli, S., Roveri, M. and Sierro, F.J.** (2013) Age refinement of the Messinian salinity crisis onset in the Mediterranean. *Terra Nova*, **25**, 315–322.
- McCave, I.N. and Langhorne, D.N.** (1982) Sand waves and sediment transport around the end of a tidal sand bank. *Sedimentology*, **29**, 95–110.
- McLean, S.R.** (1990) The stability of ripples and dunes. *Earth-Sci. Rev.*, **29**, 131–144.
- Mellere, D. and Steel, R.J.** (1996) Tidal sedimentation in Inner Hebrides half grabens, Scotland: the Mid-Jurassic Bearreraig Sandstone Formation. In: *Geology of Siliciclastic Shelf Seas* (Eds de Batist, M. and Jacobs, P.). *Geological Society of London, Special Publication*, **117**, 49–79.
- Messina, C., Nemeč, W., Martinius, A.W. and Elflein, C.** (2014) The garn formation (Bajocian-Bathonian) in the Kristin field, Halten Terrace. In: *From Depositional Systems to Sedimentary Successions on the Norwegian Continental Margin*. IAS Spec. Publ (Eds Martinius, A.W., Howell, J., Olsen, T., Ravnås, R., Steel, R.J. and Wonham, J.), Vol. **46**, pp. 513–550.
- Michaud, K.J. and Dalrymple, R.W.** (2016) Facies, architecture and stratigraphic occurrence of headland-attached tidal sand ridges in the Roda Formation, Northern Spain. In: *Contributions to Modern and Ancient Tidal Sedimentology: Proceedings of the Tidalites 2012 Conference*. Spec. Publ. Int. Ass. Sediment (Eds Tessier, B. and Reynaud, J-Y.), Vol. **47**, pp. 313–342.

- Minter, N.J., Buatois, L.A. and Mángano, M.G. (2016) The conceptual and methodological tools of ichnology. In: *The Trace-Fossil Record of Major Evolutionary Events: Volume 1: Precambrian and Paleozoic* (Eds Mángano, M.G. and Buatois, L.A.), pp. 1–26. Springer, Netherlands, Dordrecht.
- Monaco, C., Tortorici, L., Nicolich, R., Cernobori, L. and Costa, M. (1996) From collisional to rifted basins: an example from the southern Calabrian arc (Italy). *Tectonophysics*, **266**, 233–249.
- Monaco, C. and Tortorici, L. (2000) Active faulting in the Calabrian arc and eastern Sicily. *J. Geodyn.*, **29**, 407–424.
- Montenat, C., Barrier, P. and Di Geronimo, I. (1987) The Strait of Messina, past and present: a review. *Documents et Travaux IGAL*, **11**, 7–13.
- Nio, S.D. and Yang, C.S. (1991) Diagnostic attributes of clastic tidal deposits: a review. In: *Clastic Tidal Sedimentology: Calgary, Canadian Society of Petroleum Geologists* (Eds Smith, D.G., Zaitlin, B.A., Reinson, G.E. and Rahmani, R.A.), pp. 3–27.
- Olariu, C., Steel, R.J., Dalrymple, R.W. and Gingras, M.K. (2012). Tidal dunes versus tidal bars: The sedimentological and architectural characteristics of compound dunes in a tidal seaway, the lower Baronia Sandstone (Lower Eocene), Ager Basin, Spain. In: *Modern and Ancient Tidal Depositional Systems: Perspectives, Models and Signatures* (Eds Longhitano, S.G., Mellere, D. and Ainsworth, B.), *Sedimentary Geology, Special Issue*, **279**, 134–155.
- Park, S.-C., Lee, B.-H., Han, H.-S., Yoo, D.-G. and Lee, C.-W. (2006) Late quaternary stratigraphy and development of tidal sand ridges in the eastern Yellow Sea. *J. Sediment. Res.*, **76**, 1093–1105.
- Patacca, E., Sartori, R. and Scandone, P. (1990) Tyrrhenian basin and Apenninic arcs: kinematic relations since late Tortonian times. *Memorie Soc. Geol. Italiana*, **45**, 425–451.
- Patterson, R.T., Blenkinsop, J. and Cavazza, W. (1995) Planktic foraminiferal biostratigraphy and ⁸⁷Sr/⁸⁶Sr isotopic stratigraphy of the Oligocene-to-Pleistocene sedimentary sequence in the southeastern Calabrian microplate, southern Italy. *J. Paleontol.*, **69**, 7–20.
- Pedley, M. and Carannante, G. (2006) Cool-water carbonate ramps: a review. In: *Cool-Water Carbonates: Depositional Systems and Palaeoenvironmental Controls* (Eds Pedley, M. and Carannante, G.), *Geological Society, London, Special Publications*, **255**, 1–9.
- Polonia, A., Torelli, L., Mussoni, P., Gasperini, L., Artoni, A. and Klaeschen, D. (2011) The Calabrian Arc subduction complex in the Ionian Sea: Regional architecture, active deformation, and seismic hazard. *Tectonics*, **30**, TC5018.
- Pomar, L., Morsilli, M., Hallock, P. and Bádenas, B. (2012) Internal waves, an under-explored source of turbulence events in the sedimentary record. *Earth-Sci. Rev.*, **111**, 56–81.
- Posamentier, H.W. (2002). Ancient shelf ridges—a potentially significant component of the transgressive systems tract: case study from offshore northwest Java. *Am. Assoc. Petrol. Geol. Bull.* **86**, 75–106.
- Pratt, L. (1990) *The Physical Oceanography of Sea Straits*. Kluwer Academic, Dordrecht.
- Pryor, W.A., Lamborg, A.D., Roberts, M.J., Tharp, T.C. and Wilsey, W.L.M. (1990) *Geologic Controls on Porosity in Mississippian Limestone and Sandstone Reservoirs in the Illinois Basin: Chapter 22: Part I. Illinois Basin: Oil and Gas Systems. AAPG Special Volume M51: Interior Cratonic Basins*, 329–359.
- Pugh, D.T. (1987) *Tides, Surges and Mean Sea-Level*. John Wiley, New York.
- Reeder, S.L. and Rankey, E.C. (2008) Interactions between tidal flows and Ooid Shoals, Northern Bahamas. *J. Sediment. Res.*, **78**, 175–186.
- Reineck, H.E. and Singh, I.B. (1980) *Depositional Sedimentary Environments. With Reference to Terrigenous Clastics* (Springer Study Edition. Corrected Reprint of the 1st Edition). XVI, 439 S., 579 Abb., 23 Tab. Berlin–Heidelberg–New York 1975. Springer-Verlag.
- Reynaud, J.-Y. and Dalrymple, R.W. (2012) Shallow-marine tidal deposits. In: *Principles of Tidal Sedimentology* (Eds Davis R.A. and Dalrymple, B.W.), pp. 335–370. Springer, New York.
- Reynaud, J.-Y. and James, N.P. (2012) The Miocene Sommières basin, SE France: Bioclastic carbonates in a tide-dominated depositional system. *Sediment. Geol.*, **282**, 360–373.
- Reynaud, J.-Y., Tessier, B., Berné, S., Chamley, H. and Debatist, M. (1999) Tide and wave dynamics on a sand bank from the deep shelf of the Western Channel approaches. *Mar. Geol.*, **161**, 339–359.
- Rossetti, F., Faccenna, C., Goffé, B., Monié, P., Argentieri, A., Funicciello, R. and Mattei, M. (2001) Alpine structural and metamorphic signature of the Sila Piccola Massif nappe stack (Calabria, Italy): Insights for the tectonic evolution of the Calabrian Arc. *Tectonics*, **20**, 112–133.
- Rossi, V.M., Longhitano, S.G., Mellere, D., Dalrymple, R.W., Steel, R.J., Chiarella, D. and Olariu, C. (2017) Interplay of tidal and fluvial processes in an early Pleistocene, delta-fed, strait margin (Calabria, Southern Italy). *Mar. Pet. Geol.*, **1**–17.
- Rubin, D.M. (1987) Cross-bedding, bedforms, and Paleocurrents. *SEPM Concepts Sediment. Paleontol.*, **1**, 187.
- Rubin, D.M. and Hunter, R.E. (1982) Bedform climbing in theory and nature. *Sedimentology*, **29**, 121–138.
- Saha, S., Burley, S.D., Banerjee, S., Ghosh, A. and Saraswati, P.K. (2016) The morphology and evolution of tidal sand bodies in the macrotidal Gulf of Khambhat, western India. *Mar. Pet. Geol.*, **77**, 714–730.
- Saito, Y., Katayama, H., Ikehara, K., Kato, Y., Matsumoto, E., Oguri, K., Oda, M. and Yumoto, M. (1998) Transgressive and highstand systems tracts and post-glacial transgression, the East China Sea. *Sediment. Geol.*, **122**, 217–232.
- Scourse, J., Uehara, K. and Wainwright, A. (2009) Celtic Sea linear tidal sand ridges, the Irish Sea Ice Stream and the Fleuve Manche: Palaeotidal modelling of a transitional passive margin depositional system. *Mar. Geol.*, **259**, 102–111.
- Snedden, J.W. and Dalrymple, R.W. (1999) Modern shelf sand ridges: from historical perspective to a unified hydrodynamic and evolutionary model. In: *Isolated Shallow Marine Sand Bodies: Sequence Stratigraphic Analysis and Sedimentological Perspectives* (Eds Bergman, K.M. and Snedden, J.W.), *SEPM Special Publication*, **64**, 13–28.
- Snedden, J.W., Tillman, R.W. and Culver, S.J. (2011) Genesis and evolution of a mid-shelf, storm built sand ridge, New Jersey Continental Shelf, U.S.A. *J. Sediment. Res.*, **81**, 534–552.
- Surlyk, F. and Noe-Nygaard, N. (1991) Sand Bank and Dune Facies Architecture of a Wide Intracratonic Seaway: Late Jurassic-Early Cretaceous Raukelv Formation, Jameson Land, East Greenland. In: *The Three-Dimensional Facies Architecture of Terrigenous Clastic Sediments and its*

- Implications for Hydrocarbon Discovery and Recovery* (Eds Miall, A.D. and Tyler, N.), *SEPM (Society for Sedimentary Geology) Concepts in Sedimentology and Paleontology*, **3**, 261–276.
- Swift, D.J.P.** (1975) Tidal sand ridges and shoal-retreat massifs. *Mar. Geol.*, **18**, 105–133.
- Talling, P.J., Masson, D.G., Sumner, E.J. and Malgesini, G.** (2012) Subaqueous sediment density flows: Depositional processes and deposit types. *Sedimentology*, **59**, 1937–2003.
- Tansi, C., Muto, F., Critelli, S. and Iovine, G.** (2007) Neogene-Quaternary strike-slip tectonics in the central Calabrian Arc (southern Italy). *J. Geodyn.*, **43**, 393–414.
- Taylor, A.M. and Goldring, R.** (1993) Description and analysis of bioturbation and ichnofabric. *J. Geol. Soc.*, **150**, 141–148.
- Terwindt, J.H.J.** (1971) Sand waves in the southern bight of the North Sea. *Mar. Geol.*, **10**, 51–67.
- Tortorici, L., Monaco, C., Tansi, C. and Cocina, O.** (1995) Kinematics of distributed deformation in plate boundary zones with emphasis on the Mediterranean, Anatolia and Eastern Asia. Recent and active tectonics in the Calabrian arc (Southern Italy). *Tectonophysics*, **243**, 37–55.
- Tripodi, V., Muto, F. and Critelli, S.** (2013) Structural style and tectono-stratigraphic evolution of the Neogene-Quaternary Siderno Basin, southern Calabrian Arc, Italy. *Int. Geol. Rev.*, **55**, 468–481.
- Tripodi, V., Muto, F., Brutto, F., Perri, F. and Critelli, S.** (2018) Neogene-Quaternary evolution of the forearc and backarc regions between the Serre and Aspromonte Massifs, Calabria (southern Italy). *Mar. Pet. Geol.*, **95**, 328–343.
- Turco, E., Maresca, R. and Cappadona, P.** (1990) La tettonica plio-pleistocenica del confine calabro-lucano: modello cinematico. *Memorie Soc. Geol. Ital.*, **45**, 519–529.
- Van Dijk, J.P.** (1994) Late Neogene kinematics of intra-arc oblique shear zones: The Petilia-Rizzuto Fault Zone (Calabrian Arc, Central Mediterranean). *Tectonics*, **13**, 1201–1230.
- Van Dijk, J.P., Bello, M., Brancaleoni, G.P., Cantarella, G., Costa, V., Frixia, A., Golfetto, F., Merlini, S., Riva, M., Torricelli, S., Toscano, C. and Zerilli, A.** (2000) A regional structural model for the northern sector of the Calabrian Arc (southern Italy). *Tectonophysics*, **324**, 267–320.
- Vercelli, F.** (1925) *Il regime delle correnti e delle maree nello Stretto di Messina*. Commissione del Mediterraneo, Venezia.
- Visser, M. J.** (1980) Neap-spring cycles reflected in Holocene subtidal large-scale bedform deposits: a preliminary note. *Geology*, **8**(11), 543–546.
- Westaway, R.** (1993) Quaternary uplift of southern Italy. *J. Geophys. Res. Solid Earth*, **98**, 21741–21772.
- Wu, Z., Jin, X., Zhou, J., Zhao, D., Shang, J., Li, S., Cao, Z. and Liang, Y.** (2017) Comparison of buried sand ridges and regressive sand ridges on the outer shelf of the East China Sea. *Mar. Geophys. Res.*, **38**, 187–198.
- Xing, F., Wang, Y.P. and Wang, H.V.** (2012) Tidal hydrodynamics and fine-grained sediment transport on the radial sand ridge system in the southern Yellow Sea. *Mar. Geol.*, **291–294**, 192–210.
- Yang, C.-S.** (1989) Active, moribund and buried tidal sand ridges in the East China Sea and the Southern Yellow Sea. *Mar. Geol.*, **88**, 97–116.

Manuscript received 17 March 2020; revision accepted 4 January 2021